Agricultural and Forest Meteorology 388 (2026) 111286

Contents lists available at ScienceDirect

Agricultural and Forest Meteorology

journal homepage: www.elsevier.com/locate/agrformet

# Geographical and aridity gradients along with species variation shape tree growth sensitivity in the northern and southern transitional zone of China

Weipeng Yue [a,b,c], Max C.A. Torbenson [b], Feng Chen [a,c,d,e,*], Frederick Reinig [b], Jan Esper [b,f,**], Edurne Martinez del Castillo [b], Emanuele Ziaco [b], Tim Nahtz [b], Shijie Wang [a,c], Inga Kirsten Homfeld [b], Marcel Kunz [b], Xiaoen Zhao [a,c,d], Antonia Kölzer [b], Mao Hu [a,c,d], Yang Xu [a], Tiyuan Hou [a,c], Honghua Cao [a,c,d], Hechuan Wang [a], Heli Zhang [a,e], Junqiang Niu [a,c], Youping Chen [a,c]

[a] Yunnan Key Laboratory of International Rivers and Transboundary Eco-Security, Institute of International Rivers and Eco-Security, Yunnan University, Kunming, China
[b] Department of Geography, Johannes Gutenberg University, Mainz, Germany
[c] State Key Laboratory of Vegetation Structure, Functions and Construction (VegLab), Yunnan University, Kunming, China
[d] Southwest United Graduate School, Kunming, China
[e] Key Laboratory of Tree-ring Physical and Chemical Research (CMA) / Xinjiang Key Laboratory of Tree-ring Ecology, Institute of Desert Meteorology, China Meteorological Administration, Urumqi, China
[f] Global Change Research Institute of the Czech Academy of Sciences, Brno, Czech Republic

ARTICLE INFO

*Keywords:*
Tree rings
Growth response
North–South transitional zone of China
Geographical gradient
Drought gradient
Species
Forest management

ABSTRACT

Understanding the spatial distribution of tree growth sensitivity in response to climate change is essential for developing effective adaptive forest management strategies, particularly in vulnerable ecotones and transitional zones. Here, we present a network of 70 tree ring width chronologies from 12 tree species to systematically investigate the radial growth responses to key climatic factors, including temperature, precipitation, and drought (scPDSI), across the North–South transitional zone in China (NSTZ). Our analysis indicates that precipitation in the previous September ($r$ = 0.005 – 0.503), January of the current year ($r$ = 0.001 – 0.297), and late spring to early summer (April to June, $r$ = 0.003 – 0.535) exerts a positive influence on the growth of most trees (chronologies > 50), whereas temperature suppresses tree growth in May ($r$ = -0.443 – -0.004) and December ($r$ = -0.396 – -0.026) of the current year. Further redundancy (RDA) and GeoDetector (GD) analysis indicates that the spatial variability of growth sensitivity is primarily governed by combined geographic, aridity gradients, and species, with local microclimatic variables such as vapor pressure deficit (VPD) and soil moisture exerting comparatively weaker influences. Multi-model projections under the SSP2–4.5 and SSP5–8.5 scenarios suggest that the transitional zone is likely to experience a drier and increasingly heterogeneous eco-climatic regime (the mean coefficient of variation > 0.25). Such changes may intensify the spatial divergence and potential destabilization of tree growth–climate relationships, posing challenges for forest ecosystem long-term sustainability.

## 1. Introduction

Forest ecosystems play a critical role in maintaining ecological balance, conserving the environment, and supporting sustainable development of human societies (Führer, 2000; Perry et al., 2008; Watson et al., 2018). As their principal components, trees directly determine the structure and functional patterns of forest ecosystems, act as a link in the circulation of matter and energy, and deeply couple complex ecological processes (Bardgett et al., 2014; Maynard et al., 2022; Waring and Running, 2010). Current climate change has seriously impacted the structure, composition and function of forest ecosystems, particularly through the increased frequency and intensity of drought, which have significantly altered the physiological processes and growth dynamics of trees, causing increased tree mortality and severe forest decline,

* Corresponding author at: Yunnan Key Laboratory of International Rivers and Transboundary Eco-Security, Institute of International Rivers and Eco-Security, Yunnan University, Kunming, China.
** Corresponding author at: Department of Geography, Johannes Gutenberg University, Mainz, Germany.
*E-mail addresses:* feng653@163.com (F. Chen), esper@uni-mainz.de (J. Esper).

https://doi.org/10.1016/j.agrformet.2026.111286
Received 16 September 2025; Received in revised form 21 May 2026; Accepted 29 May 2026

challenging forest management and threatening supply of forest ecosystem services (Liu et al., 2013b; Martinez del Castillo et al., 2022; Williams et al., 2013; van Mantgem et al., 2009; Gao et al., 2018; Clark et al., 2016; McDowell et al., 2020). Notably, differences in functional traits, water-use strategies, and carbon allocation among tree species lead to inconsistent growth response patterns (King et al., 2013; Trugman et al., 2019). Understanding how trees respond to climate variability is thus vital for projecting future forest dynamics and formulating adaptive management strategies (Millar et al., 2007).

Tree rings provide a high-resolution temporal record of forest ecosystems, with tree-ring width (TRW) being highly sensitive to climate variability, thus providing valuable insights into both historical climate–growth relationships and potential future trajectories (Babst et al., 2014; Chen et al., 2026; De Micco et al., 2019; Huang et al., 2010; Wilmking et al., 2020). While numerous studies have explored tree growth–climate relationships, most have been conducted at limited spatial scales involving a few sites or species, which hinders the identification of complex and heterogeneous response patterns (He et al., 2013; Vitali et al., 2017; Zang et al., 2012; Yue et al., 2024a). Furthermore, studies investigating the spatial heterogeneity of growth response patterns along geographic spatial gradients and driving factors are limited to relatively uniform forest types or narrow ecological backgrounds, such as temperate forests in the north and subtropical forests in the south, which may not fully reveal the complexity and instability of climate-growth relationships in highly diverse forest ecosystems (Altmanová et al., 2025; Li et al., 2020, 2023b; Su et al., 2021). In regions such as ecological transition zones, which are characterized by substantial variation in ecosystem composition, climatic fluctuations, and physiological strategies, tree responses to climate may exhibit pronounced nonlinearity (Albrich et al., 2020; Charney et al., 2016; Grimm et al., 2013). For instance, forest ecosystems located in humid to semi-humid regions or along the subtropical–temperate boundary often display heightened interannual sensitivity and increased responsiveness to extreme events (Jentsch and von Heßberg, 2022; Li et al., 2023a; Liu et al., 2013a; Xie et al., 2024a). There is a pressing need, therefore, to analyze dendrochronological datasets encompassing a wide range of climate zones, ecosystem types, and species assemblages.

The North–South transitional zone in China (NSTZ) serves as a critical interface in both natural and cultural geography (Fig. 1). It reflects sharp gradients in moisture, temperature, and agricultural practices ranging from humid to arid, from warm to cold, and from paddy to dryland farming systems (Li et al., 2021; Zhang et al., 2021; Zhu and Lu,

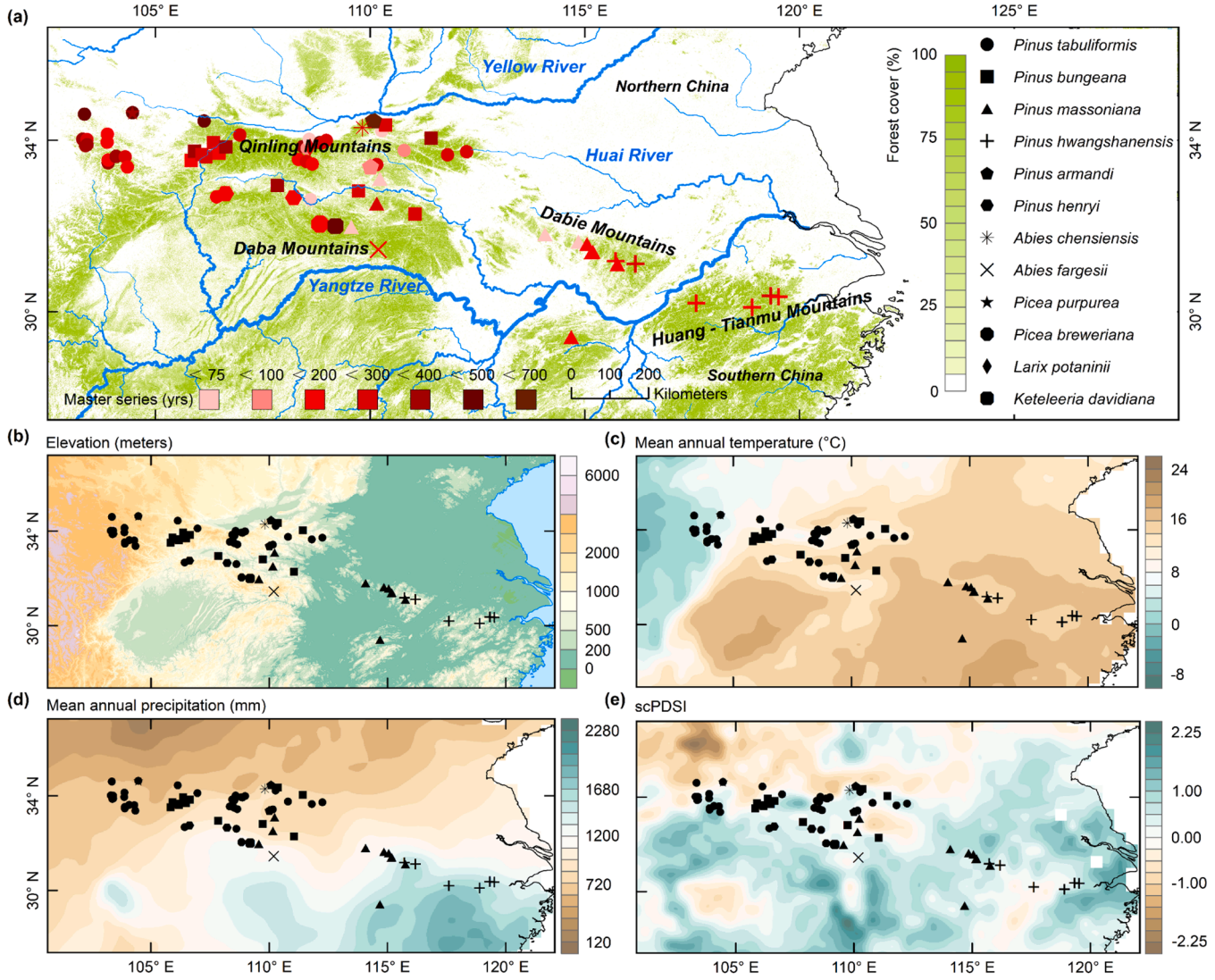


**Fig. 1.** Geographic and climatic patterns of the North–South Transitional Zone in China (NSTZ). (a) Spatial extent of the NSTZ, forest cover (Hansen et al., 2013), and 70 tree ring width chronologies. The Qinling Mountains–Huai River Line represents both the geographical boundary between northern and southern China and the core axis of the NSTZ. (b) – (e) Spatial elevation, annual temperature, precipitation, and self-calibrating Palmer Drought Severity Index (scPDSI) patterns (1950 – 2022).

2025). As a confluence of northern and southern climate regimes, this region is particularly sensitive to global climate change and represents an ideal natural laboratory for monitoring and evaluating forest ecosystem dynamics and climate responses (Li et al., 2023a). Although dendroclimatological studies have been conducted in this region, most have focused on individual sites or a limited number of species (Cai et al., 2020; Ma et al., 2025; Peng et al., 2025; Wang et al., 2022; Yan et al., 2020). Here, we establish a multi-species TRW chronology network across an extensive east–west and north–south climatic gradient within the NSTZ (Fig. 1). This network enables us to comprehensively investigate the relationship between tree growth and climate variability. The objectives of this study are to: (1) explore the radial growth response trees to major climate elements; (2) analyze the key factors driving changes in response sensitivity.

## 2. Materials and methods

### 2.1. Study area overview

The NSTZ is derived from the concept of the geographical demarcation line defined by the Qinling Mountains–Huai River boundary. At the level of macroscopic expressions such as landscape patterns and living customs, the NSTZ concentrates the superposition and convergence of China's north–south differences; whereas in large-scale climatic and topographic patterns, a pronounced northwest–southeast gradient predominates (Fig. 1). Along the northwest–southeast direction, the regional climate shifts gradually from humid subtropical conditions in the south to warm temperate conditions in the north, exhibiting marked changes in temperature and precipitation patterns (He and Hao, 2024). Correspondingly, vegetation types display a clear latitudinal zonation, with subtropical evergreen broad-leaved forests and mixed evergreen–deciduous broad-leaved forests dominating the south and transitioning northward into warm temperate deciduous broad-leaved forests, while conifer–broadleaf mixed forests occur at higher elevations in mountainous areas (Kou et al., 2020). Concurrently, soil types exhibit a distinct transitional pattern aligned with climate and vegetation, with red and yellow soils prevailing in the southern hilly and mountainous regions and gradually giving way to brown and cinnamon soils in northern mountainous areas, while alluvial (fluvisol) and other cultivated soils are widespread across the plains (Shi et al., 2004). The NSTZ is primarily governed by the East Asian monsoon system, under which hydrothermal conditions exhibit substantial variability at interannual to decadal timescales (Wang et al., 2021; Yue et al., 2026). The distinct transitional features of this region, encompassing a broad spectrum of geographic and climatic gradients, provide an excellent opportunity for investigating the spatial variability of climate-growth relationships.

### 2.2. Tree-ring data

To capture the longitudinal and latitudinal gradients along the NSTZ, we employed a large-scale sampling strategy encompassing 128 sites and 1735 trees, resulting in 3457 increment cores (including 130 cores from 89 trees at five sites archived in the ITRDB) (Fig. 1 and Table S1). The sampling focused on conifer species from five genera namely *Pinus, Larix, Picea, Abies*, and *Keteleeria*, including 12 key species: *Pinus tabuliformis, Pinus bungeana, Pinus massoniana, Pinus hwangshanensis, Pinus armandi, Pinus henryi, Picea purpurea, Larix potaninii, Abies chensiensis, Picea breweriana* (i.e., *Picea brachytyla*), *Keteleeria davidiana*, and *Abies fargesii* (Table S1). Pure conifer stands dominate most sites, though some contain mixtures with deciduous broadleaf species such as *Betula* and *Quercus*, as well as evergreen broadleaf species including *Cyclobalanopsis* and *Rhododendron*, alongside shrubs from families including Caprifoliaceae, Rosaceae, Vitaceae, and Fabaceae. Many of the sampled conifers represent the local upper or lower latitudinal limits of their species, such as *Pinus tabuliformis, Pinus bungeana* and *Picea breweriana* south of the Daba Mountains, and *Keteleeria davidiana* to the north. Certain forests are fragmented due to anthropogenic disturbances, and for these we integrated nearby samples with similar stand characteristics (e.g., HLB and TJYS) based on species composition and proximity (Yue et al., 2024b) (Table S1). Ultimately, we constructed 70 robust site chronologies with sufficient sample replication for dendrochronological analysis (sample size $> 10$) (Fig. 2).

All cores were air-dried, mounted, and sanded (Speer, 2010). Older samples were visually cross-dated under a binocular microscope and measured using the Velmex measuring system (Final year $< 2019$) (Chen et al., 2023; Cook and Kairiukstis, 2013) (Table S1). More recent samples were scanned at a minimum resolution of 2400 DPI using an EPSON scanner, and ring widths were measured from high-resolution images using CooRecorder 9.4 (Maxwell et al., 2021). Both approaches ensured a measurement precision of 0.001 mm. Cross-dating accuracy and measurement quality were assessed using the COFECHA program (Holmes, 1983; Chen et al., 2024b; Grissino-Mayer, 2001). Most series were detrended using the Friedman variable-span smoother (alpha = 5) (Friedman, 1984; Cook, 1986), a non-parametric adaptive local regression technique suitable for datasets from forest interiors where tree competition and disturbance are substantial (Allen et al., 2015) (Table S1 and Fig. S1). For two sites, the Friedman smoother failed to capture growth trends and was subsequently substituted with a 67% smoothing spline (site BYS) or a negative exponential curve ($K > 0$) (site ZYG) (Biondi and Qeadan, 2008; Cook and Peters, 1981). All detrending and standardization procedures were conducted using the ARSTAN program (Cook, 1986). Tree-ring width series were first divided by fitted growth curves to remove age-related trends. Variance stabilization was achieved via Rbar-weighted standardization (Rbar: average correlation between tree-ring sequences). We computed 50-year moving-window correlations (with a 25-year overlaps) to assess common signal strength and constructed standardized chronologies by calculating bi-weight robust means of the standardized series (STD) (Yue et al., 2024b). To evaluate the strength of the climate signal in each chronology, we also calculated statistical indices such as the autoregressive model of order 1 (AR1), the expressed population signal (EPS), the signal-to-noise ratio (SNR), the variance in first eigenvector (VFE), and mean sensitivity (MS) (Esper et al., 2002) (Figs. 2 and S2) (Table S2).

### 2.3. Environmental data

The environmental datasets employed in this study are categorized into two main groups: geospatial variables and climatic variables. Geospatial data for each sampling site include recorded values of longitude (Lon), latitude (Lat), elevation (Ele), and the mean length of series (MLS, representing the age structure of the sampled trees; see Table S1). For sites composed of consolidated, spatially scattered samples, the final geospatial values were derived by averaging all recorded values prior to integration. Climatic variables encompass both macro-scale background climate indicators and localized environmental factors. The macro-scale variables, namely mean temperature (Tem), total precipitation (Pre), and the self-calibrating Palmer Drought Severity Index (scPDSI), were extracted from the CRU 4.08 with a spatial resolution of $0.5^\circ \times 0.5^\circ$ (Harris et al., 2020). In contrast, local-scale climatic indicators such as vapor pressure deficit (VPD), soil moisture (Soil-m), and climatic water deficit (CWD) were sourced from the TerraClimate gridded dataset, which provides high-resolution data at $1/24^\circ \times 1/24^\circ$ (Abatzoglou et al., 2018). This resolution is particularly well-suited for capturing microclimatic variability and spatial heterogeneity at the site level. While climate gridded datasets provide an efficient and widely adopted representation of climatic variables, caution is warranted when applying them to small-scale or local studies (New et al., 2002). For all climate variables, site-specific monthly values were extracted using a point-to-point matching method. Long-term mean values for the period 1958 – 2022 were then computed to represent the prevailing local climate conditions at each sampling site (macro-scale variables calculation for the period 1950 – 2022). To further characterize moisture

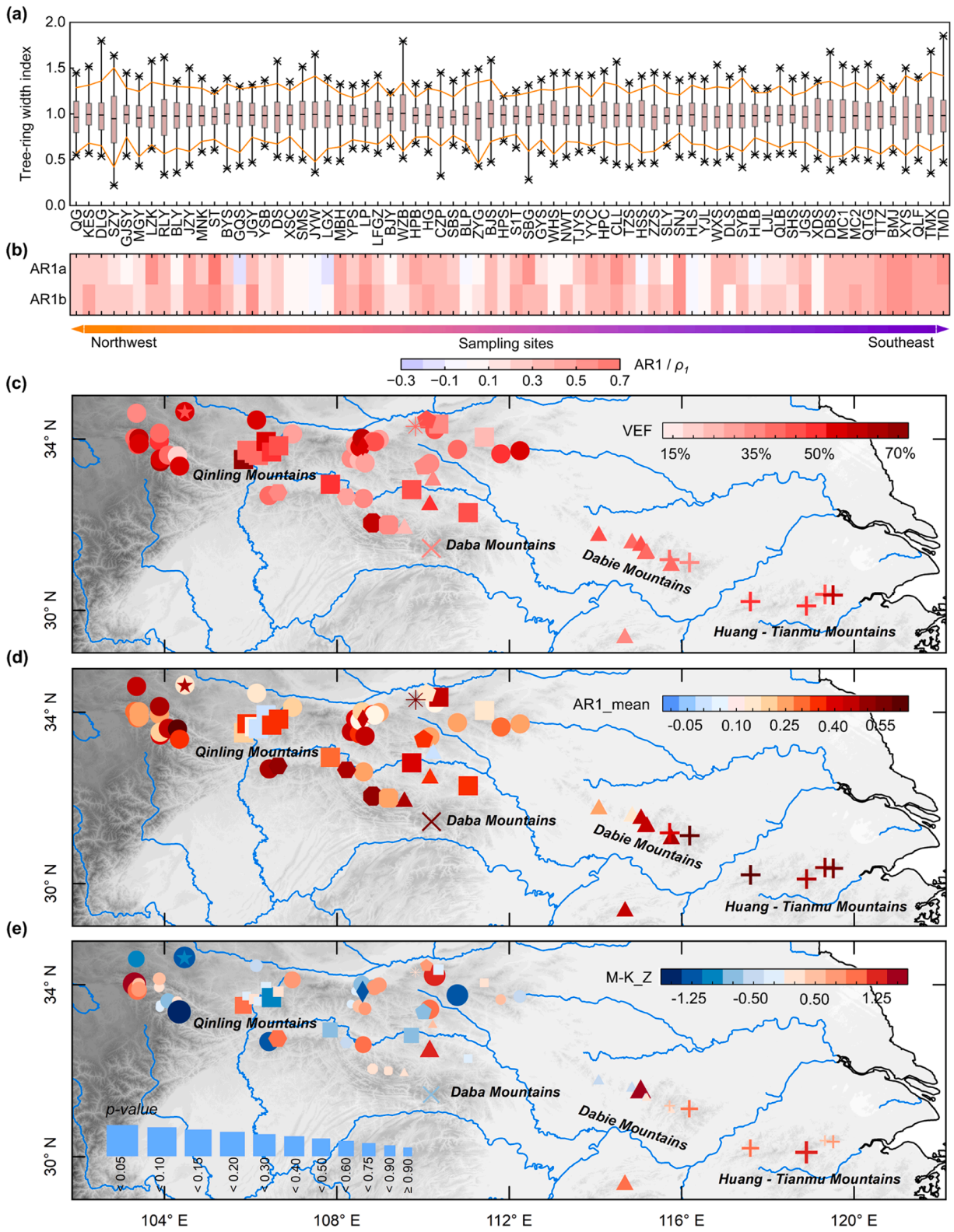


**Fig. 2.** Distribution characteristics and long-term trends of 70 tree-ring chronologies along the North–South Transitional Zone in China (NSTZ). (a) Boxplots illustrating the distribution of tree-ring width indices, where boxes represent the interquartile range (25th –75th percentiles), whiskers indicate the 1st – 99th percentiles, and the 5th – 95th percentiles are shown by connecting lines. Chronology names are ordered from northwest to southeast according to their spatial distribution. (b) Heatmaps showing the first-order autoregressive (AR1) coefficients of each chronology, calculated for two evaluation periods (AR1a since 1950 and AR1b since the EPS $\geq$ 0.85 cutoff year) (Table S2). (c) – (e) Maps displaying the variance explained by the first eigenvector (VFE), mean first-order autoregressive coefficients (AR1a and AR1b), and Mann–Kendall (M–K) Z statistics of growth trends for each chronology during 1950 – 2022, respectively. For the M–K Z statistics, blue colors indicate decreasing trends, whereas red colors indicate increasing trends. The significance of the trends (p values) is represented by symbol size. Different symbol shapes denote different tree species, and detailed classifications are provided in Fig. 1a.

availability gradients across sites, we derived two widely used aridity indices based on different methodological frameworks: the UNEP (United Nations Environment Programme) Aridity Index (U-AI) and the De Martonne aridity index (De M-AI: Budyko, 1961; de Martonne, 1926). Given the scarcity and limited reliability of instrumental climate records prior to the 1950s in the NSTZ, we restricted our analysis to the period from 1950 to 2022, which aligns with the temporal coverage of most sampling sites (Fig. S2). To extend the future climate perspective for the NSTZ, we further employed multi-model ensemble means from 24 CMIP6 simulations (Coupled Model Intercomparison Project Phase 6), including historical runs and future projections under two Shared Socioeconomic Pathways: a moderate mitigation scenario (SSP2–4.5) and a high-emission, fossil fuel–dependent scenario (SSP5–8.5) (for similar procedure see Chen et al., 2024a) (Table S3).

### 2.4. Statistical methods

We employed Pearson correlation analysis to evaluate the relationships between tree-ring radial growth and conventional climatic variables (Lo et al., 2010). Specifically, we calculated site-level correlation coefficients between standardized tree-ring width chronologies and corresponding climatic parameters over their overlapping years. Given that tree growth often exhibits physiological lag effects and legacy responses, we incorporated both the 12 months of the previous year (P) and the 12 months of the current year (C) into a 24-month temporal window for analysis (Kannenberg et al., 2019). To enhance spatial representativeness and comparability, we included all chronologies in the analysis, even those with series shorter than 50 years. To identify the environmental variables that exert the strongest influence on climate–-growth relationships, we performed redundancy analysis (RDA) using an interactive forward selection procedure (ter Braak, 1986; Dixon, 2003). In this analysis, the 24-month correlation coefficients of temperature, precipitation, and scPDSI with tree growth served as response variables, while geospatial, climatic variables, and tree species types were treated as explanatory variables. During RDA, the relative contributions of the predictors were ranked, and their significance was assessed through Monte Carlo permutation tests. The results were visualized using biplots to reveal patterns in multivariate space. Tree species were dummy-coded (0/1) to avoid subjective weighting. To prevent perfect multicollinearity, *Picea breweriana* was selected as the reference level, as it is an extremely small population and only a single sampling site. This approach ensures model estimability while retaining all biological information within the RDA framework. Although RDA is a classic constrained ordination technique well-suited for identifying linear associations and synergistic effects among environmental drivers, it is inherently limited by its reliance on linear assumptions and covariance structures (Fig. S2). These limitations may reduce its explanatory power in contexts characterized by strong spatial heterogeneity or non-linear interactions (Altmanová et al., 2025). To address this, we incorporated the GeoDetector (GD) method as a complementary approach (Wang et al., 2016; Song et al., 2020). Unlike RDA, the GD framework does not assume linearity and instead quantifies the explanatory power of individual and interacting variables from the perspective of spatial stratified heterogeneity. As with RDA, we used the 24-month climate–growth correlation coefficients as response variables and calculated the q statistic to quantify the explanatory power of each factor. Higher q values indicate stronger explanatory power. Continuous predictors were discretized into four strata using the quantile method to facilitate stratified analysis. Subsequently, we constructed linear models to link the most influential variables identified by both methods to the climate–growth sensitivity metrics for temperature, precipitation, and drought. We further applied analysis of variance to assess whether their climate sensitivity trends vary along the gradients of key environmental drivers (Su et al., 2021; Altmanová et al., 2025).

## 3. Results

### 3.1. Chronology statistics and growth variability

The sampled forests were predominantly composed of natural stands ranging from middle-aged to near old-growth, with a mean chronology length of 126.9 years and relatively stable long-term growth trajectories (Table S1). Tree growth at most sampling sites exhibited high sensitivity to climate, with mean MS values close to 0.21, but pronounced regional differences were observed (Table S2). The overall sample set effectively captured a coherent climatic signal, as indicated by mean VFE values exceeding 40% (Fig. 2) (Table S2). The sampling design represented the regional population signal well, with an overall EPS of 0.927 (Table S2). AR1 across the two evaluation periods (since 1950 and since the EPS $\geq$ 0.85 cutoff year) ranged between -0.18 and 0.63, with most chronologies exhibiting moderate autocorrelation (ranged between 0.09 and 0.41) (Fig. 2) (Table S2). VFE and AR1 values displayed the same spatial distribution pattern, characterized by a decrease from the northwest toward the central Qinling–Daba Mountains, followed by an increase southeastward toward the Dabie Mountains (Fig. 2). Over the past 70 years, tree-ring width indices at all sampling sites fluctuated around a mean value of 0.98, with an interquartile range of approximately 0.90 – 1.20. Growth variability differed among species, and Mann–Kendall trend tests indicated predominantly increasing growth trends at eastern sites, whereas trends at central and western sites were more heterogeneous; however, none of these trends were statistically significant (Fig. 2).

### 3.2. Tree growth responses to major climatic variables

Monthly temperature, precipitation, and scPDSI from previous and current year were used for analyzing radial growth responses. Overall, the growth–climate relationships across all sampling sites exhibit pronounced heterogeneity across seasons, tree species, and geographical regions (Figs. 3 and S3). Regarding temperature sensitivity, most sites within the NSTZ exhibit negative correlations with mean temperature during the current growing season (May – August) and winter (December). These negative responses are primarily observed in *Pinus tabuliformis* and *Pinus bungeana* (Fig. S3). Spatially, they are more pronounced in the western region than in the central and eastern regions, where the correlations are mostly insignificant (Fig. 3). Positive correlations with temperature are primarily observed from the Daba and Dabie Mountains to areas south of the Yangtze River, particularly in *Pinus hwangshanensis, Pinus massoniana*, and *Pinus henryi*, and are concentrated in early winter to spring (January – March) and the previous summer (June – July). Correlations with precipitation indicate that tree growth at most sampling sites is significantly and positively related to spring precipitation (April – May) (Fig. 3). This sensitivity decreases progressively from the northwest to southeast and becomes insignificant in the Dabie Mountains and further east. Significant positive correlations with previous-year September precipitation are observed primarily in *Pinus tabuliformis, Pinus bungeana*, and *Keteleeria davidiana* (Fig. S3). In contrast, many sites east of the Qinling and Daba Mountains exhibit significant negative correlations with previous summer (May – August) precipitation, especially among *Pinus massoniana* and *Pinus hwangshanensis*. Compared to the complex growth responses to temperature and precipitation, tree growth responses to drought are more spatially and taxonomically consistent. Positive correlations are mainly concentrated between the previous year May and the current year September, with the strongest correlations significance during the current growing season (May – September) (Fig. 3). This pattern is evident at most sites, except for a few dominated by *Pinus hwangshanensis, Abies chensiensis, Abies fargesii*, and a small number of *Pinus massoniana*. Within the 25th to 75th percentile range of correlation coefficients (entirely on one side of either positive or negative) tree growth shows predominantly negative correlations with temperature in May (*r*

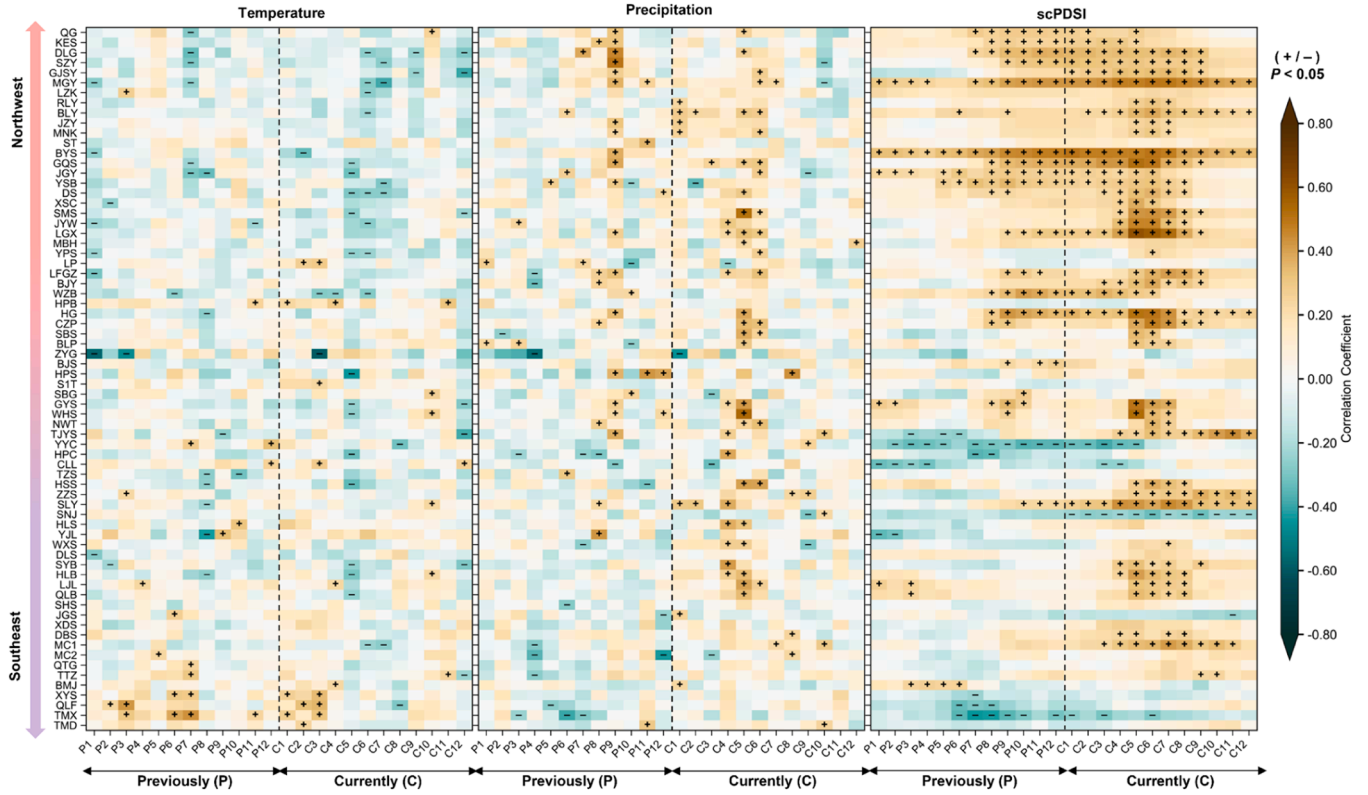


**Fig. 3.** Site-by-site Pearson correlations between tree-ring width (TRW) chronologies and major climatic variables (temperature, precipitation, and scPDSI) across 70 sites in the North–South Transitional Zone of China (NSTZ). The y-axis indicates the spatial distribution of sampling sites, arranged along a northwest–southeast gradient. Tree species classification follows the order shown in Fig. S3. The x-axis represents a 24-month period from previous-year January (P1) to the current-year December (C12), with the black dashed lines denoting annual boundaries. Symbols "+" and "–" indicate statistically significant positive and negative correlations, respectively.

= -0.201 – -0.021) and December ($r$ = -0.195 – -0.032); predominantly positive correlations with precipitation in the previous September ($r$ = 0.006 – 0.234), April ($r$ = 0.036 – 0.214), May ($r$ = 0.048 – 0.272), and June ($r$ = 0.020 – 0.208); and predominantly positive correlations with scPDSI in all months except March (Fig. S4).

### 3.3. Variations in growth–climate relationships along environmental gradients

In the model based on scPDSI, RDA1 alone accounted for 72.89% of the total variance, significantly outperforming the other two models, indicating that scPDSI, as an integrated indicator of moisture availability, has the strongest explanatory power for tree growth. Further variance partitioning showed that Lon, Lat, Ele, U-AI, De M-AI, Tem, Pre, CWD, MLS, *Pinus tabuliformis, Pinus bungeana, Pinus hwangshanensis, Pinus armandi* and *Pinus henryi* all contributed significantly ($p < 0.05$) to at least one of the climate-growth models. However, only Lon, De M-AI, and MLS were consistently significant across all three models, with longitude exhibiting highly significant explanatory power in all cases ($p < 0.001$), particularly in the scPDSI-based model. By summing the explained variation for each explanatory variable across the three RDA models, the cumulative contributions of Lon, De M-AI, and Lat were higher than those of the other variables (Figs. 4 and S5; Table S4).

The results of the factor detector analysis based on the GD method are shown in Fig. 5. Explanatory variables with high explanatory power (q-values) and frequent statistical significance across the 24-month period included Lon, Lat, Ele, Tem, Pre, U-AI, De-M AI, and tree species. For temperature-growth relationships, the most influential months were previous year January and July, the late winter to early spring (November – March), and the mid-summer to autumn period (July – November). For precipitation-growth relationships, key months included previous year January, the autumn–winter period (September – December), and the early growing season (March – July), as well as October of the current year. For drought-growth relationships, the main period of sensitivity spanned from previous May to current September. Integrating results from both analyses, we found that Lon and the De-M AI exert the strongest control over the spatial heterogeneity in tree growth sensitivity, acting as the dominant drivers of spatial variation in growth-climate responses across the NSTZ. Meanwhile, explanatory variables such as MLS, Lat, Ele, Tem, Pre, U-AI, and tree species also play important roles. Notably, both RDA and GD consistently indicated that localized climatic variables such as VPD, Soil-m, and CWD had relatively weak and mostly non-significant explanatory power.

Based on the angular relationships and vector lengths in RDA, together with the GD results, we observed strong sensitivity gradients in the response of tree growth to climate across three specific temporal windows: January – March, May – June, and previous May – current September (Fig. 6). Specifically, the sensitivity of tree radial growth to temperature increased linearly with Lon, Tem, Pre, De-M AI, and U-AI, while decreasing linearly along Lat, Ele, and MLS gradients. All these fitted relationships reached statistical significance ($p < 0.05$), with the exception of MLS. Among the six major groups comprising the 12 tree species, temperature sensitivity exhibited a general upward trend, with *Pinus hwangshanensis* displaying the highest overall sensitivity. Conversely, the sensitivity of radial growth to precipitation and drought (scPDSI) showed an inverse pattern, decreasing linearly with Lon, Tem, Pre, De-M AI, and U-AI, but increasing along Lat, Ele, and MLS gradients. All fitted relationships were statistically significant ($p < 0.05$), except for the correlation between precipitation sensitivity and Ele. Across the species types, moisture sensitivity demonstrated a general downward trend, with *Pinus tabuliformis* exhibiting the highest overall sensitivity to water availability. These gradient changes collectively reflect the spatial

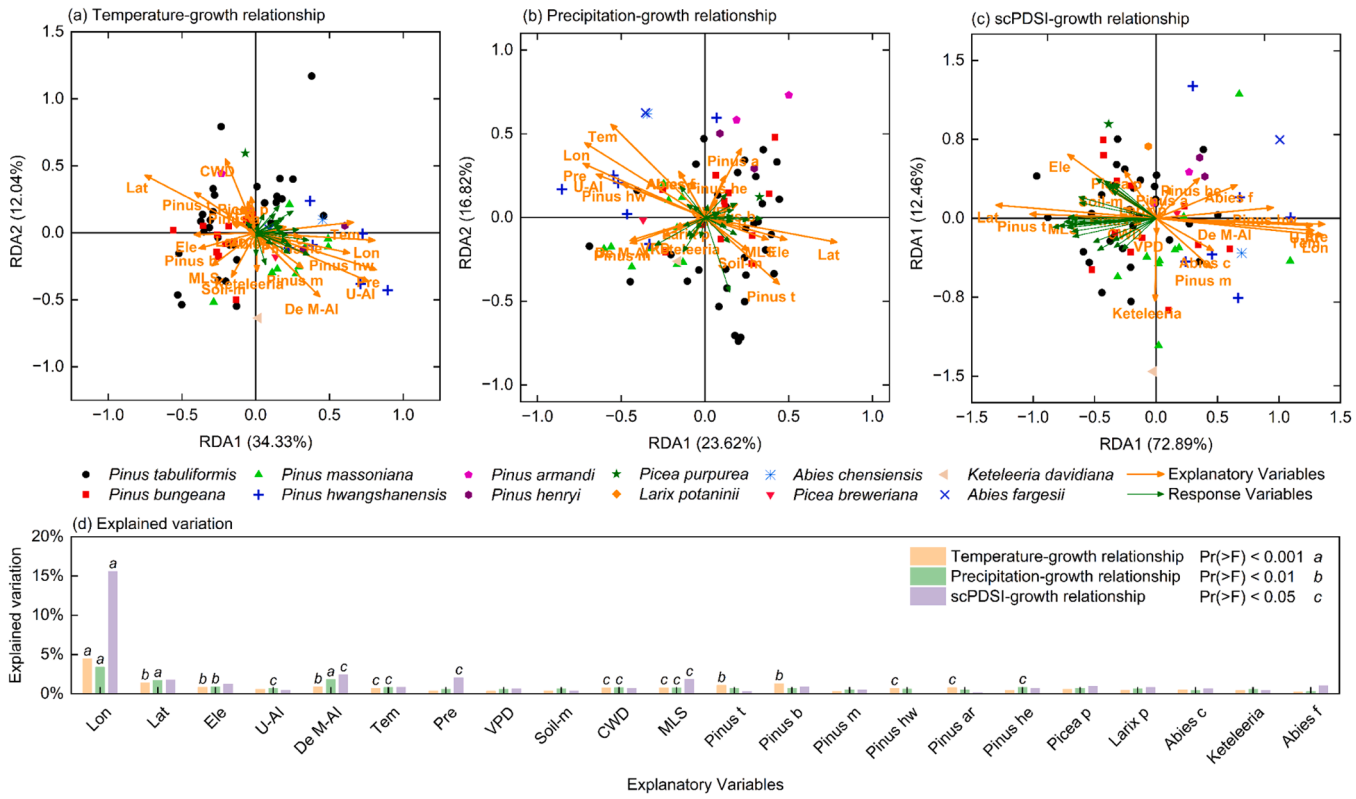


**Fig. 4.** Redundancy analysis (RDA) biplots of tree growth–climate response relationships across the North–South transitional zone (NSTZ). (a) to (c) detail the growth responses to temperature, precipitation, and scPDSI, respectively. The approximate correlation between explanatory variables (22 explanatory variables, including geographic features, climatic conditions, and tree species types, are represented by orange vectors) and response variables (correlation coefficients for 24 monthly windows across 70 sites, shown as green vectors) is indicated by the cosine of the angle between vectors: acute, obtuse, and right angles denote positive, negative, and near-zero correlations, respectively. (d) shows the proportion of variance explained by each of the 22 explanatory variables of the three growth–climate response models. The labels *Pinus t, Pinus b, Pinus m, Pinus hw, Pinus ar, Pinus he, Picea p, Larix p, Abies c, Keteleeria*, and *Abies f* are abbreviations of the following tree species: *Pinus tabuliformis, Pinus bungeana, Pinus massoniana, Pinus hwangshanensis, Pinus armandi, Pinus henryi, Picea purpurea, Larix potaninii, Abies chensiensis, Keteleeria davidiana*, and *Abies fargesii*, respectively.

pattern of the sensitivity of radial tree growth in the NSTZ to major climatic factors. In warm and humid low-elevation areas, where *Pinus hwangshanensis* and *Pinus massoniana* dominate, tree growth is more sensitive to temperature, typically showing positive correlations, while responses to precipitation and drought signals are relatively weak. In contrast, in drier regions, tree growth exhibits stronger positive correlations with moisture availability, particularly with precipitation and drought indices (Fig. 7).

## 4. Discussion

### 4.1. Spatial variations in growth–climate relationships

Across the 70 sampling sites in the NSTZ, both the structural properties of the chronologies and the growth trends exhibit clear spatial differentiation (Fig. 2) (Table S2). A systematic assessment of radial growth responses to temperature, precipitation, and the scPDSI also reveals clear regional differentiation variability (Figs. 3 and S4). Trees in the northwest exhibit significant negative correlations with temperatures from May to September, possibly due to increased evapotranspiration under high temperatures, which intensifies soil drought, restricts fine root water uptake, and reduces xylem transport efficiency (Brunner et al., 2015; Choat et al., 2018; Meinzer et al., 2001). In contrast, trees in the southeast show enhanced positive responses to winter–spring (January – March) temperatures, likely because warmer winters facilitate earlier dormancy release and cambial reactivation in early spring (Maurya and Bhalerao, 2017; Way, 2011). Precipitation shows predominantly positive effects on growth during late spring and early summer (April – June), although its significance diminishes from northwest to southeast. This gradient reflects structural differences in regional water supply–demand relationships, which directly regulate tree growth through moisture availability and drought stress. In the semi-humid northwest, moisture is a limiting factor, and interannual variability in precipitation directly affects cambial activity and xylem cell production (Gao et al., 2019; Zhao et al., 2019a), making drought stress the dominant constraint on growth and increasing tree sensitivity to water availability. In contrast, in the humid southeast, where precipitation is abundant, water is no longer the primary limiting factor, and excessively wet conditions may even impair physiological activity, resulting in negative effects (Cai and Liu, 2017; Cai et al., 2017; Cai et al., 2024). Collectively, the positive effects of precipitation in the previous September, January, and the early growing season (April – June) on radial growth across the NSTZ likely reflect the importance of soil moisture recharge and legacy effects in regulating cambial activity (Gheyret et al., 2021; Yan et al., 2026; Henttonen et al., 2014). By contrast, elevated temperatures in May and December may reduce carbon availability for current or subsequent growth by constraining photosynthesis and carbon assimilation (Dusenge et al., 2019; Körner, 2003). Together, these findings highlight the synergistic roles of water availability and temperature-driven physiological stress in shaping radial growth variability.

By analyzing how tree growth–climate sensitivity varies across the NSTZ under the modulation of geographic and local climatic conditions, we find that spatial gradients and aridity gradients are the primary and statistically significant drivers of spatial heterogeneity in growth sensitivity (Figs. 4 and 5) (Table S5). However, these geographic variables

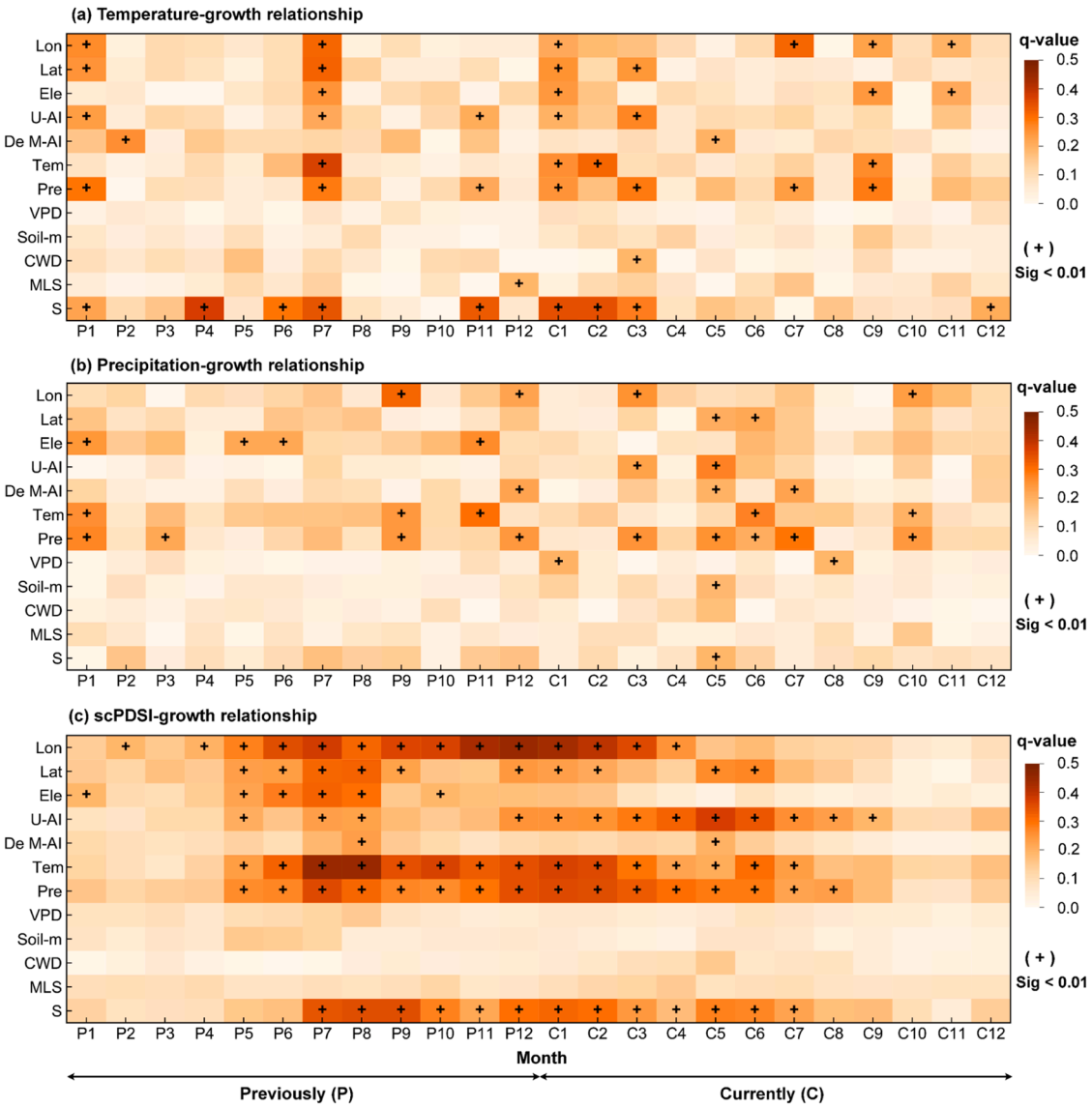


**Fig. 5.** Geographical factor detector (GD) results of three tree growth–climate response models across the North–South transitional zone (NSTZ). (a) to (c) detail the growth responses to temperature, precipitation, and scPDSI, respectively. The vertical axis represents the explanatory variables, where S is the abbreviation for tree species and the full names corresponding to the other abbreviated labels are provided in Fig. 4. The horizontal axis represents the response variables, with P1 to C12 indicating the correlation coefficients between tree growth and climate over 24 months, from the previous year to the current year. The q-value indicates the explanatory power of each individual factor on the response variable, with symbols "+" denoting statistical significance at $p < 0.01$.

representing spatial gradients should be interpreted as proxies for underlying climatic gradients rather than direct drivers of tree growth (Martin-Benito et al., 2015; Altman et al., 2017). In this context, longitude and latitude primarily reflect large-scale variations in temperature and moisture regimes, while elevation is closely associated with temperature decline, changes in atmospheric conditions, and potential shifts in moisture availability (Mountain Research Initiative EDW Working Group, 2015; Xie et al., 2024b; Sidor et al., 2015). Therefore, the observed spatial patterns likely reflect variations in temperature regimes, moisture availability, and drought stress across the region. Generally, longitude and latitude represent the macroscopic direction of changes in water and heat. The sensitivity of tree growth to climate factors often undergoes quasi-linear succession along these two dimensions, reflecting the spatial expression of the gradual adaptation and restriction mechanism of trees to water and heat factors (Briffa et al., 2004; Esper et al., 2002; Fritts, 2012; Lyu et al., 2017). For example, in the forest–steppe ecotone of southern Siberia, *Pinus sylvestris* exhibits pronounced drought sensitivity, with climate exerting stronger control over growth in the west than in the east (Tabakova et al., 2020). Similarly, tree-ring networks in northern forests of northeastern China demonstrate that radial growth limitations due to differences in climate vary along the latitudinal gradient (Li et al., 2020). Our results support these general findings and further reveal an even more pronounced linear gradient along the longitudinal dimension.

The De M-AI, a simple yet integrative indicator of moisture conditions, offers a robust spatial metric for characterizing regional hydrothermal coupling and is widely used as a background variable to assess tree growth dynamics (Bhuyan et al., 2017; Martinez del Castillo et al., 2022; Su et al., 2021). For instance, *Pinus latteri* in southern Laos exhibits lower growth resistance and higher recovery capacity under drier (lower De M-AI) conditions, while in wetter areas (higher De M-AI), recovery components show no significant differences (Gao et al., 2025). On the Yunnan–Guizhou Plateau in southwestern China, climate sensitivity of subtropical conifers increases along the De M-AI gradient (Su et al., 2021). In Europe and Mediterranean forests, growth tends to respond to short- and medium-term droughts, whereas forests in continental

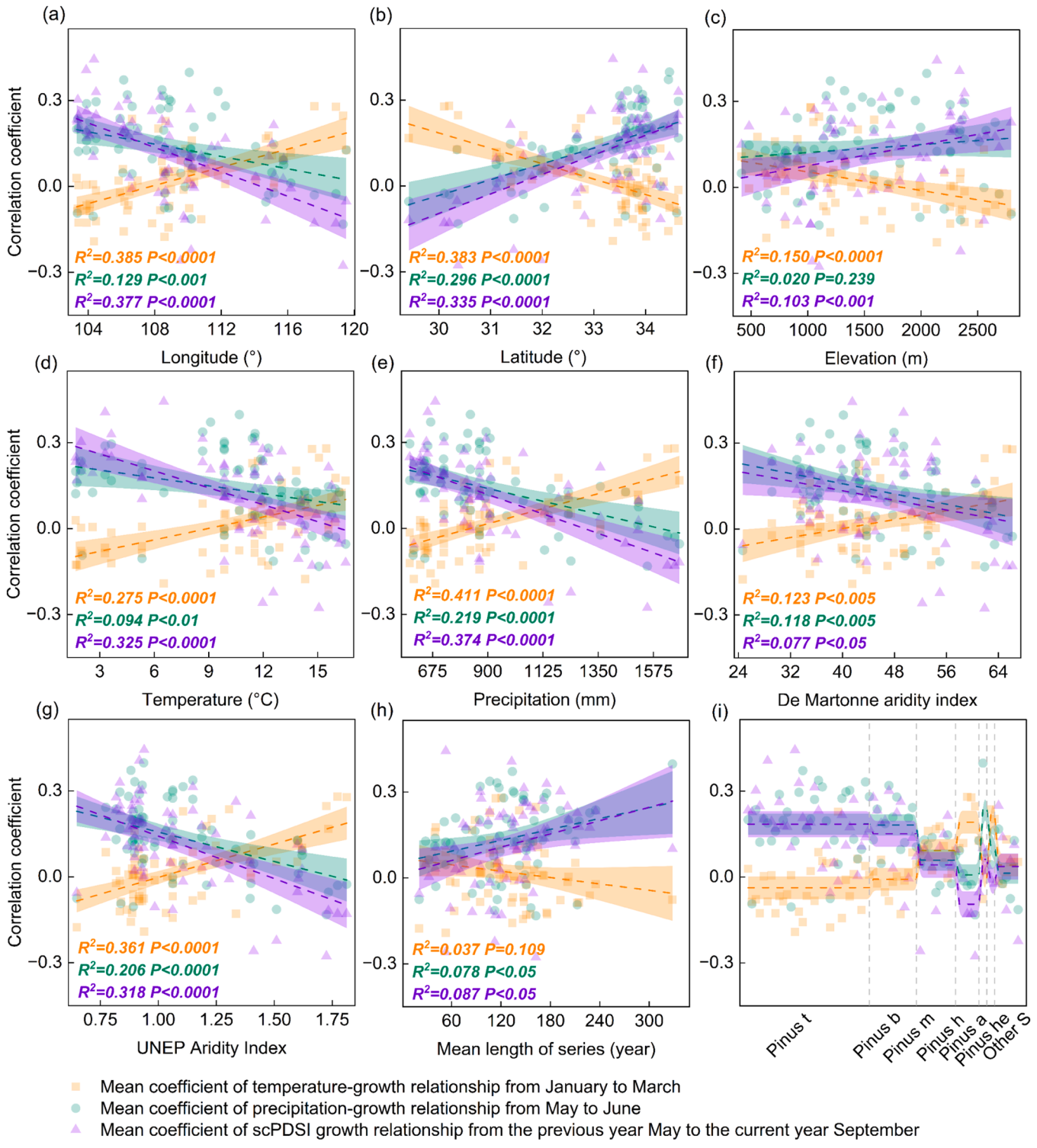


**Fig. 6.** Gradient variations in the mean sensitivity of tree radial growth responses to temperature, precipitation, and scPDSI along longitude (a), latitude (b), elevation (c), temperature (d), precipitation (e), De Martonne aridity index (f), UNEP Aridity Index (g), mean length of series (h), and tree species (i). (a) to (h) show the linear relationships between the mean response sensitivity and each explanatory variable. The strength of linear relationships is indicated by the coefficient of determination ($R^2$), significance level ($P$), and 95% two-sided confidence intervals (shaded areas: orange for temperature response, green for precipitation response, and purple for scPDSI response). (i) illustrates the variation in mean response sensitivity among tree species. The dashed line represents the mean value calculated for each species group, and the shaded area denotes the error of 0.5 standard deviations, with colors matching those used in the linear fits above. The x-axis tick labels correspond to tree species, and the full names of the abbreviations can be found in Fig. 4. "Other S" denotes species represented by only one chronology, including *Picea purpurea, Larix potaninii, Abies chensiensis, Picea breweriana, Keteleeria davidiana*, and *Abies fargesii*.

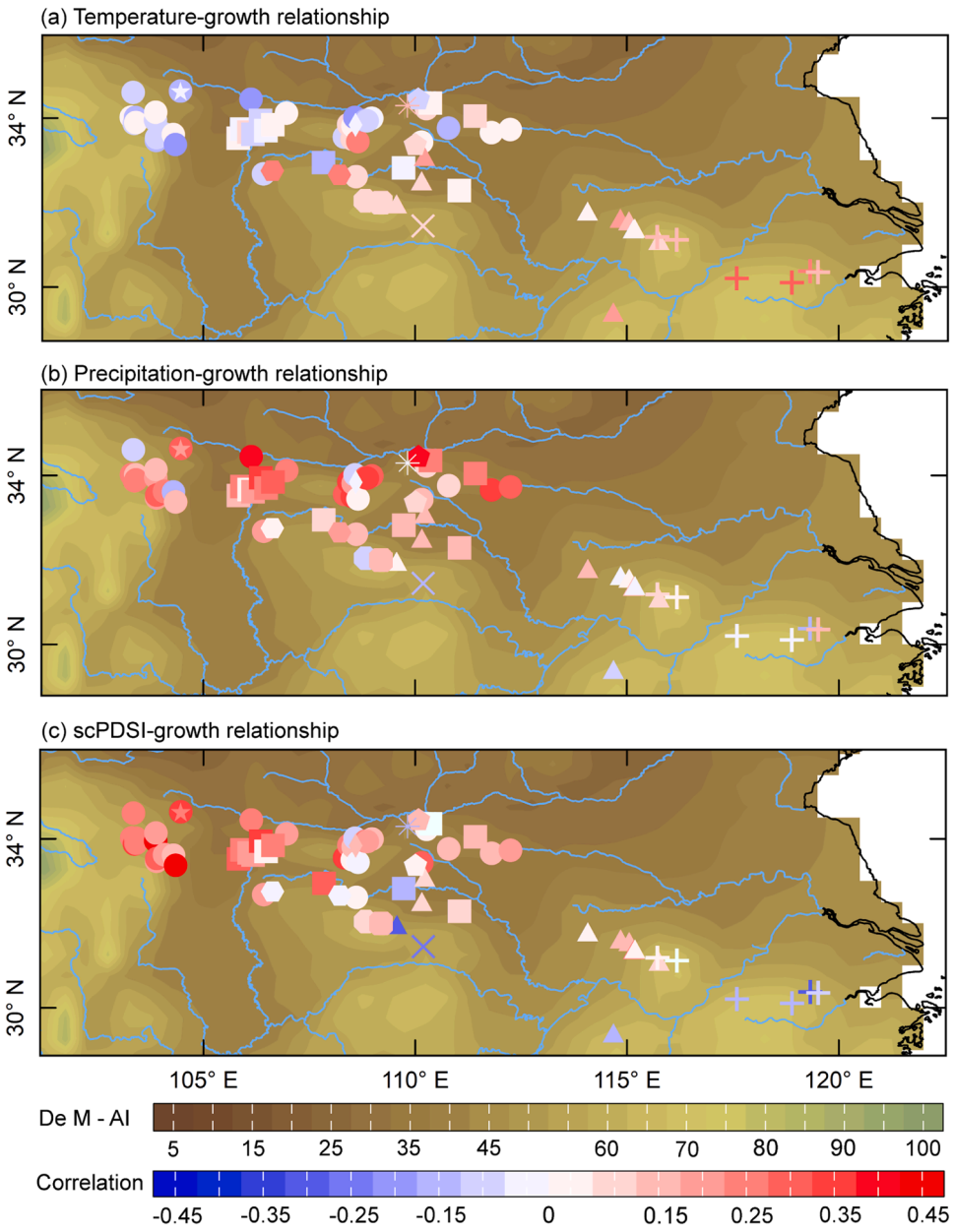


**Fig. 7.** Spatial distribution of the sensitivity of radial tree growth to major climatic factors in the North–South transitional zone in China. (a) Correlation coefficients between radial tree growth and temperature (mean temperature from January to March). (b) Correlation coefficients between radial tree growth and precipitation (mean precipitation from May to June). (c) Correlation coefficients between radial tree growth and scPDSI (mean scPDSI from May of the previous year to September of the current year). The base map displays the long-term climatology of the De Martonne aridity index (De-M AI), categorized by index levels. Different symbol shapes denote different tree species; detailed classifications are provided in Fig. 1a.

climates exhibit stronger drought tolerance and can withstand long-term droughts (Bhuyan et al., 2017). This evidence suggests that aridity gradients not only shape spatial patterns of tree growth dynamics but also reflect ecological resilience and adaptive strategies to climate variability. We observed divergent explanatory capacities of the De M-AI and the U-AI in RDA and GD analyses. This discrepancy may result from their differing formulations: the De M-AI is more sensitive to temperature and better captures transitional gradients, whereas the U-AI emphasizes evaporative demand and is better suited to spatial zonation (Ullah et al., 2022). Nevertheless, both indices consistently identify aridity as a key driver of spatial heterogeneity in tree-ring–climate sensitivity across the NSTZ. Overall, these results suggest that spatial heterogeneity in growth–climate sensitivity across the NSTZ is primarily driven by direct ecological factors, particularly drought stress, whereas geographic variables largely serve as integrative proxies for the underlying environmental gradients.

### 4.2. Species effects on growth–climate relationships

Different tree species across the NSTZ also exhibit pronounced differences in their growth and in their responses to environmental variability. For instance, *Pinus tabuliformis, Pinus bungeana*, and *Pinus hwangshanensis* exhibit greater fluctuations in ring-width indices, indicating heightened sensitivity to interannual environmental variability (Chen et al., 2024c; Huang et al., 2021; Li et al., 2024; Liang et al., 2019; Xie et al., 2024; Zhao et al., 2021). In contrast, *Abies* and *Picea* exhibit more stable growth at certain sites, potentially due to their conservative ecological strategies and relatively stable habitats (Cavin et al., 2013;

Fuchs et al., 2021). *Pinus bungeana* and *Pinus tabuliformis*, known for their high drought tolerance and adaptability, show pronounced negative responses to high temperatures and positive responses to spring precipitation in the northwest, reflecting their sensitivity to hot–dry stress (Cao et al., 2025; Chen et al., 2024c; Peng et al., 2023; Xie et al., 2024). *Pinus massoniana* and *Pinus hwangshanensis* exhibit strong positive correlations with winter–spring temperatures, suggesting that these subtropical conifers rely on warm conditions to initiate early-spring growth (Li et al., 2024; Meng et al., 2021). However, their responses to summer temperature or drought are not consistent, indicating more complex sensitivities to hydrothermal interactions (Chen et al., 2016; Wang et al., 2019). Different *Abies* species also display highly divergent responses to temperature and moisture. *Abies chensiensis* is sensitive to winter temperatures, while *Abies fargesii* shows significant responses to autumn precipitation, likely due to differences in elevational distribution (Chen et al., 2015; Dang et al., 2007). Similarly, *Picea purpurea* and *Picea breweriana* exhibit temporal shifts in climate response windows, suggesting that *Picea* are more heat-sensitive and that their northern distribution is constrained by temperature thresholds (Zhao et al., 2019c). Notably, species *Keteleeria davidiana* all exhibit significant responses to both precipitation and drought during autumn and early winter, indicating a late-season water-use strategy that may provide insights into forest adaptation mechanisms under future climate change (Yue et al., 2024b; Zhao et al., 2019b).

These interspecific differences in radial growth characteristics and climate–response relationships are also key drivers of the sensitivity gradients observed across the NSTZ. In the integrated RDA and GD analyses, the tree species variable explained a substantial proportion of the variance, suggesting that species identity plays an important role in shaping the observed patterns. Systematic differences among tree species in hydraulic architecture, wood density, rooting depth, stomatal regulation strategies, and phenological schedules may lead to divergent sensitivities to temperature, moisture availability, and extreme climatic events (Oliveira et al., 2021; Roderick and Berry, 2001; Brum et al., 2017; Chen et al., 2022; Pau et al., 2011). Meanwhile, the spatial distribution of tree species in the NSTZ is constrained by geographic and climatic gradients, further magnifying tree species effects on growth–climate relationships. This interplay between tree species composition and climatic gradients creates pronounced spatial differentiation in growth–climate relationships across the NSTZ, further reinforcing the heterogeneity of climate response sensitivity. It should be noted that the traits of tree species under different climatic conditions may be affected by potential regional environmental gradients (Vilà-Cabrera et al., 2015; McKown et al., 2014). Therefore, when analyzing their climate response sensitivity, the results should be interpreted with caution in conjunction with specific regional differences.

### 4.3. Implications for future forest management

The heterogeneous responses of trees to climatic factors in the NSTZ are not only the result of current ecological adaptation but also reflect the selective pressures experienced during their evolutionary history. Regional variations in response patterns indicate that forests in different areas may face distinct climate-related risks. For instance, forests in the northwestern part of the NSTZ are more prone to compound stress from elevated temperatures and drought, whereas southeastern regions may increasingly face risks of premature budburst and late spring frost due to warmer winters. Inter-species differences in climate response suggest the need to implement spatially heterogeneous management strategies for future forest management and restoration in the NSTZ (Baskent et al., 2024; Seidl et al., 2018). Based on CMIP6 multi-model ensemble simulations and projections of the De-M AI, the NSTZ has remained relatively humid and climatically stable over the past century. However, projections suggest that the climatic conditions at the 70 chronology sites are projected to undergo dramatic shifts in the future (Fig. 8 and Table S4). Under the high-emission scenario SSP5–8.5, projected average

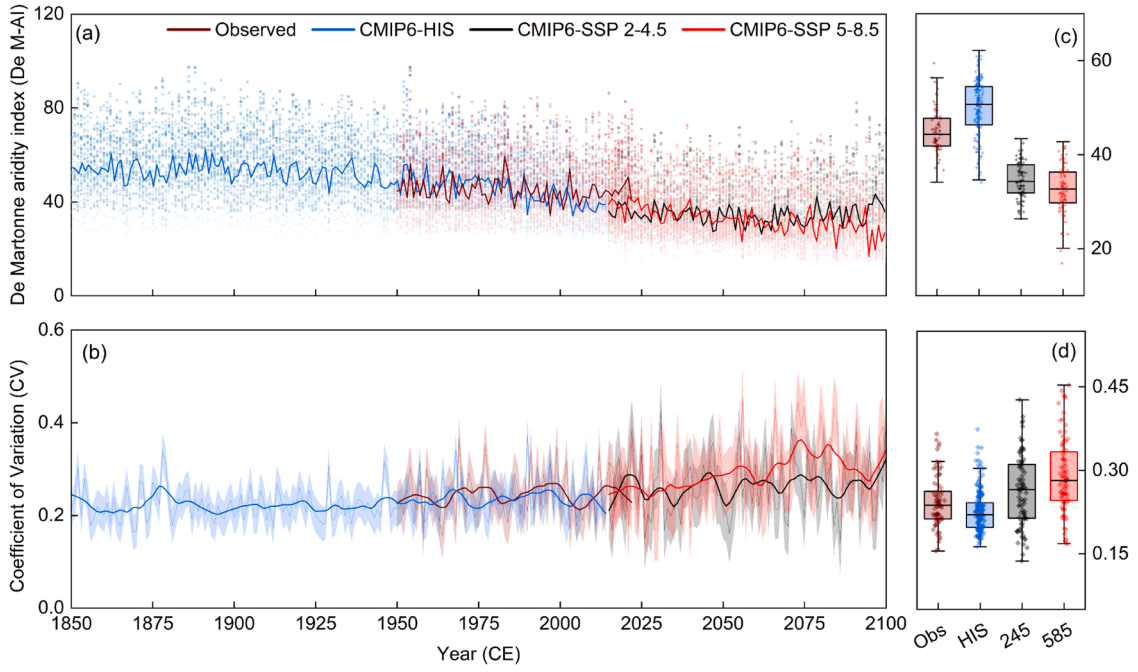


**Fig. 8.** Changes and variability of the De Martonne aridity index at 70 chronology sites based on observations, model simulations, and future projections. (a) Temporal evolution of the De Martonne aridity index derived from observations (Observed, 1950 – 2022, purple), historical simulations from CMIP6 multi-model ensemble means (CMIP6–HIS, 1850 – 2014, blue), and future projections under SSP2–4.5 (black) and SSP5–8.5 (red) scenarios (2015 – 2100). All curves represent averages across the 70 chronology sites. Boxplots on the right (c) show the distribution (25th – 75th percentile) of mean index values for each period. (b) Coefficient of variation of the De Martonne aridity index for the observational period, historical simulations, and future projections. Shaded bands represent ±1 standard deviation, and all series are smoothed using a 10-year low-pass filter. Boxplots on the right (d) display the distribution (25th – 75th percentile) of the coefficient of variation across each period.

aridity levels approach the historical lower bound, suggesting that the region may transition toward a drier and more variable ecological-climatic regime. Given the observed relationship between aridity gradients and tree growth–climate sensitivity in this study, such projected drying trends are likely to enhance drought stress and increase the sensitivity of tree growth to moisture availability, particularly in already water-limited regions, potentially leading to reduced growth stability (Mirabel et al., 2023; Wang et al., 2025; Wu et al., 2025). In extreme cases, previously observed drought-gradient effects could be altered, with potential shifts in response patterns over time. These projections highlight the urgent need for adaptive innovation in forest ecological research and management strategies (Hagerman and Pelai, 2018; Wilson and Cagalanan, 2016). In regions expected to experience significant aridification, priority should be given to the introduction and conservation of drought-tolerant native tree species (Fuchs et al., 2021). Additionally, optimizing forest stand structure to enhance the buffering capacity of ecosystems will be critical for responding more scientifically and effectively to the vulnerabilities and transitions associated with uncertain future climate risks (Wagner et al., 2014).

### 4.4. Limitations and perspectives

Some microenvironmental variables, such as CWD, VPD, and Soil-m did not show strong contributions in our analyses. However, this does not imply these factors are irrelevant to tree growth (Altmanová et al., 2025) (Figs. 4 and 5). Instead, their weak explanatory power may stem from their limited spatiotemporal synchrony, which hinders stable signal transfer into tree-ring width chronologies (Mirabel et al., 2023; Tumajer et al., 2022). CWD reflects the balance between water and energy availability in ecosystems and is often aligned with short-term climatic extremes (Altmanová et al., 2025). VPD, a key instantaneous driver of evapotranspiration, exhibits high-frequency fluctuations and low interannual stability (Asbjornsen et al., 2011). Soil moisture is strongly influenced by local soil types, vegetation cover, and micro-topography, making it difficult to capture its role through meteorological reanalysis alone (Su et al., 2021). Consequently, these factors may not show robust associations with long-term growth sensitivity patterns. Future research should systematically integrate high-resolution, in situ micro-environmental observations to enhance the explanatory power of these factors in growth–climate analyses. Our analysis also finds that the MLS significantly contributes to both temperature and drought sensitivity estimates (Fig. 6). This implies that chronology length should be treated as a covariate in growth–climate sensitivity assessments. However, given the non-uniform spatial construction of sample networks, variations in sample number and length may confound spatial gradients (Fig. S2). Therefore, strict data quality control is essential, and caution should be exercised when interpreting such findings (Speer, 2010; Pan et al., 2011). In addition, the spatial coverage of sampling sites and the representativeness of sampled species should be expanded in the NSTZ, particularly by increasing the proportion of diverse angiosperms.

## 5. Conclusions

Based on 70 tree-ring width chronologies in the NSTZ, this study systematically analyzed the relationship between radial growth and main climatic factors, including temperature, precipitation, and drought, the driving mechanisms behind the changes in growth sensitivity, and the potential impacts under future climate change using CMIP6 multi-model climate projections. We found that the response of tree-ring radial growth to climate exhibits significant species-specific and spatial heterogeneity in the NSTZ. Precipitation generally exert positive influences on tree growth during spring and summer, while temperature shows a negative effect in early summer and winter. However, such response relationships are not consistent across regions and tree species, reflecting a typical pattern of response heterogeneity. The redundancy and GeoDetector analysis jointly indicate that changes in growth sensitivity in the NSTZ are mainly shaped by the combined effects of geographic location, aridity gradient, and tree species, while local microclimatic variables such as vapor pressure deficit and soil moisture are not closely related. According to CMIP6 multi-model ensemble projections, the NSTZ will shift toward a drier and more variable ecological-climatic state in the future, which may intensify the differentiation of ecosystem vulnerability and lead to the disappearance of existing gradient effects in growth sensitivity. The findings of this study have important implications for forest management and ecological adaptation strategies in the NSTZ.

## Code availability

The code used to analyze data is available from the corresponding author upon request.

## CRediT authorship contribution statement

**Weipeng Yue:** Writing – review & editing, Writing – original draft, Visualization, Validation, Supervision, Software, Resources, Project administration, Methodology, Investigation, Funding acquisition, Formal analysis, Data curation, Conceptualization. **Max C.A. Torbenson:** Writing – review & editing, Visualization, Resources, Methodology, Formal analysis, Conceptualization. **Feng Chen:** Writing – review & editing, Supervision, Resources, Project administration, Investigation, Funding acquisition, Data curation. **Frederick Reinig:** Writing – review & editing, Visualization, Software, Methodology, Formal analysis, Conceptualization. **Jan Esper:** Writing – review & editing, Visualization, Supervision, Software, Resources, Methodology, Formal analysis, Conceptualization. **Edurne Martinez del Castillo:** Writing – review & editing, Visualization, Methodology, Formal analysis. **Emanuele Ziaco:** Writing – review & editing, Visualization, Formal analysis. **Tim Nahtz:** Writing – review & editing, Visualization, Software, Conceptualization. **Shijie Wang:** Writing – review & editing, Visualization, Methodology, Investigation, Data curation. **Inga Kirsten Homfeld:** Writing – review & editing, Visualization, Formal analysis. **Marcel Kunz:** Writing – review & editing, Visualization, Formal analysis. **Xiaoen Zhao:** Writing – review & editing, Visualization, Investigation, Data curation. **Antonia Kölzer:** Writing – review & editing, Visualization, Formal analysis. **Mao Hu:** Writing – review & editing, Visualization, Investigation, Data curation. **Yang Xu:** Writing – review & editing, Investigation, Data curation. **Tiyuan Hou:** Writing – review & editing, Investigation, Data curation. **Honghua Cao:** Writing – review & editing, Investigation, Data curation. **Hechuan Wang:** Investigation, Data curation. **Heli Zhang:** Writing – review & editing, Investigation, Data curation. **Junqiang Niu:** Investigation, Data curation. **Youping Chen:** Writing – review & editing, Investigation, Data curation.

## Declaration of competing interest

The authors declare that they have no known competing financial interests or personal relationships that could have appeared to influence the work reported in this paper.

## Acknowledgements

This study was supported by Excellent Research Group Program for Tibetan Plateau Earth System (No. 42588201), the National Natural Science Foundation of China (No. 32061123008), the China Scholarship Council (202407030045), and the Scientific Research and Innovation Project of Postgraduate Students in the Academic Degree of Yunnan University (KC-23233869). We are grateful to researchers who have shared tree-ring width data via the International Tree-Ring Data Bank (ITRDB).

## Supplementary materials

Supplementary material associated with this article can be found, in the online version, at doi:10.1016/j.agrformet.2026.111286.

## Data availability

The tree-ring response sensitivity results can be downloaded from the Mendeley Data Repository Center (DOI: 10.17632/y7g25wjm9d.1). Climate data can be obtained from the Climatic Research Unit (https://crudata.uea.ac.uk/cru/data/hrg/) and TerraClimate (https://www.climatologylab.org/terraclimate.html), respectively. The CMIP6 datasets are accessible at Earth System Grid Federation website (https://esgf-node.llnl.gov/search/cmip6/).

## References


Abatzoglou, J.T., Dobrowski, S.Z., Parks, S.A., Hegewisch, K.C., 2018. TerraClimate, a high-resolution global dataset of monthly climate and climatic water balance from 1958 to 2015. Sci. Data 5 (1), 170191.

Albrich, K., Rammer, W., Seidl, R., 2020. Climate change causes critical transitions and irreversible alterations of mountain forests. Glob. Change Biol. 26 (7), 4013–4027.

Allen, K.J., Nichols, S.C., Evans, R., Cook, E.R., Allie, S., Carson, G., Ling, F., Baker, P.J., 2015. Preliminary December–January inflow and streamflow reconstructions from tree rings for western Tasmania, southeastern Australia. Water Resour. Res. 51 (7), 5487–5503.

Altman, J., Fibich, P., Santruckova, H., Dolezal, J., Stepanek, P., Kopacek, J., Hunova, I., Oulehle, F., Tumajer, J., Cienciala, E., 2017. Environmental factors exert strong control over the climate-growth relationships of Picea abies in Central Europe. Sci. Total Environ. 609, 506–516.

Altmanová, N., Fibich, P., Doležal, J., Bažant, V., Černý, T., Molina, J.G.A., Enoki, T., Hara, T., Hoshizaki, K., Ida, H., Janda, P., Kagawa, A., Kopecký, M., Korznikov, K.A., Krestov, P.V., Kubota, Y., Lanta, V., Macek, M., Mejstřík, M., Nakamura, M., Noguchi, M., Omelko, A.M., Petřík, P., Sakai, T., Song, J.S., Suzuki, S.N., Svoboda, M., Šrůtek, M., Treydte, K., Ukhvatkina, O.N., Ulbrichová, I., Vozmishcheva, A.S., Wang, X., Altman, J., 2025. Spatial heterogeneity of tree-growth responses to climate across temperate forests in Northeast Asia. Agric. For. Meteorol. 362, 110355.

Asbjornsen, H., Goldsmith, G.R., Alvarado-Barrientos, M.S., Rebel, K., Van Osch, F.P., Rietkerk, M., Chen, J., Gotsch, S., Tobón, C., Geissert, D.R., Gómez-Tagle, A., Vache, K., Dawson, T.E., 2011. Ecohydrological advances and applications in plant–water relations research: a review. J. Plant Ecol. 4 (1–2), 3–22.

Babst, F., Alexander, M.R., Szejner, P., Bouriaud, O., Klesse, S., Roden, J., Ciais, P., Poulter, B., Frank, D., Moore, D.J.P., Trouet, V., 2014. A tree-ring perspective on the terrestrial carbon cycle. Oecologia 176 (2), 307–322.

Bardgett, R.D., Mommer, L., De Vries, F.T., 2014. Going underground: root traits as drivers of ecosystem processes. Trends Ecol. Evol. 29 (12), 692–699 (Amst.).

Baskent, E.Z., Borges, J.G., Kašpar, J., 2024. An updated review of spatial forest planning: approaches, techniques, challenges, and future directions. Curr. For. Rep. 10 (5), 299–321.

Bhuyan, U., Zang, C., Menzel, A., 2017. Different responses of multispecies tree ring growth to various drought indices across Europe. Dendrochronologia 44, 1–8 (Verona).

Biondi, F., Qeadan, F., 2008. A theory-driven approach to tree-ring standardization: defining the biological trend from expected basal area increment. Tree Ring Res. 64 (2), 16.

Briffa, K.R., Osborn, T.J., Schweingruber, F.H., 2004. Large-scale temperature inferences from tree rings: a review. Glob. Planet. Change 40 (1), 11–26.

Brum, M., Teodoro, G.S., Abrahao, A., Oliveira, R.S., 2017. Coordination of rooting depth and leaf hydraulic traits defines drought-related strategies in the campos rupestres, a tropical montane biodiversity hotspot. Plant Soil 420 (1), 467–480.

Brunner, I., Herzog, C., Dawes, M.A., Arend, M., Sperisen, C., 2015. How tree roots respond to drought. Front. Plant Sci. 6, 2015.

Budyko, M.I., 1961. The heat balance of the Earth's surface. Sov. Geogr. 2 (4), 3–13.

Cai, Q., Liu, Y., 2017. Two centuries temperature variations over subtropical southeast China inferred from Pinus taiwanensis Hayata tree-ring width. Clim. Dyn. 48 (5), 1813–1825.

Cai, Q., Liu, Y., Liu, H., Sun, C., Wang, Y., 2017. Growing-season precipitation since 1872 in the coastal area of subtropical southeast China reconstructed from tree rings and its relationship with the East Asian summer monsoon system. Ecol. Indic. 82, 441–450.

Cai, Q., Liu, Y., Qian, H., Liu, R., 2020. Inverse effects of recent warming on trees growing at the low and high altitudes of the Dabie Mountains, subtropical China. Dendrochronologia 59, 125649 (Verona).

Cai, Q., Xie, M., Liu, Y., Fang, C., Hao, Z., Ren, M., Zhou, Q., Mu, Y., Chen, Y., 2024. The influence of North Atlantic sea surface temperature fluctuations on the climate of the Qinling-Bashan Mountains, China based on a 250 year tree-ring record. Palaeogeogr. Palaeoclimatol. Palaeoecol. 649, 112320.

Cao, H., Chen, F., Hu, M., Hou, T., Zhao, X., Wang, S., Zhang, H., 2025. Tree-Ring insights into past and future streamflow variations in Beijing, Northern China. Water Resour. Res. 61, e2024WR038084.

Cavin, L., Mountford, E.P., Peterken, G.F., Jump, A.S., 2013. Extreme drought alters competitive dominance within and between tree species in a mixed forest stand. Funct. Ecol. 27 (6), 1424–1435.

Charney, N.D., Babst, F., Poulter, B., Record, S., Trouet, V.M., Frank, D., Enquist, B.J., Evans, M.E.K., 2016. Observed forest sensitivity to climate implies large changes in 21st century North American forest growth. Ecol. Lett. 19 (9), 1119–1128.

Chen, Y., Chen, F., Hu, M., Zhao, X., Cao, H., Wang, S., Esper, J., Büntgen, U., Torbenson, M.C.A., Hou, T., Xu, H., Lin, Y., 2026. Unprecedented recent summer warming and cross-sphere hydrological coupling in Asian Water Towers. NPJ Clim. Atmos. Sci. 9, 6.

Chen, D., Fang, K., Li, Y., Dong, Z., Zhang, Y., Zhou, F., 2016. Response of Pinus taiwanensis growth to climate changes at its southern limit of Daiyun Mountain, mainland China Fujian Province. Sci. China Earth Sci. 59 (2), 328–336.

Chen, F., Man, W., Wang, S., Esper, J., Meko, D., Büntgen, U., Yuan, Y., Hadad, M., Hu, M., Zhao, X., Roig, F., Fang, O., Chen, Y., Zhang, H., Shang, H., Yu, S., Luo, X., He, D., Chen, F., 2023. Southeast Asian ecological dependency on Tibetan Plateau streamflow over the last millennium. Nat. Geosci. 16 (12), 1151–1158.

Chen, F., Wang, S., Dong, Q., Esper, J., Büntgen, U., Meko, D., Linderholm, H.W., Wang, T., Yue, W., Zhao, X., Hadad, M., González-Reyes, Á., Chen, F., 2024a. Role of Pacific Ocean climate in regulating runoff in the source areas of water transfer projects on the Pacific Rim. NPJ Clim. Atmos. Sci. 7 (1), 153.

Chen, F., Wang, T., Zhao, X.E., Esper, J., Ljungqvist, F.C., Büntgen, U., Linderholm, H.W., Meko, D., Xu, H.N., Yue, W.P., Wang, S.J., Yuan, Y.J., Zheng, J.Y., Pan, W., Roig, F., Hadad, M., Hu, M., Wei, J.C., Chen, F.H., 2024b. Coupled Pacific Rim megadroughts contributed to the fall of the Ming Dynasty's capital in 1644 CE. Sci. Bull. 69 (19), 3106–3114 (Beijing).

Chen, F., Zhang, R.B., Wang, H.Q., Qin, L., 2015. Recent climate warming of central China reflected by temperature-sensitive tree growth in the eastern Qinling Mountains and its linkages to the Pacific and Atlantic oceans. J. Mt. Sci. 12 (2), 396–403.

Chen, S., Wei, W., Huang, Y., 2024c. Biophysical controls on canopy transpiration of Pinus tabulaeformis under different soil moisture conditions in the Loess Plateau of China. J. Hydrol. 631, 130799.

Chen, Z., Li, S., Wan, X., Liu, S., 2022. Strategies of tree species to adapt to drought from leaf stomatal regulation and stem embolism resistance to root properties. Front. Plant Sci. 13, 926535.

Choat, B., Brodribb, T.J., Brodersen, C.R., Duursma, R.A., López, R., Medlyn, B.E., 2018. Triggers of tree mortality under drought. Nature 558 (7711), 531–539.

Clark, J.S., Iverson, L., Woodall, C.W., Allen, C.D., Bell, D.M., Bragg, D.C., D'Amato, A. W., Davis, F.W., Hersh, M.H., Ibanez, I., Jackson, S.T., Matthews, S., Pederson, N., Peters, M., Schwartz, M.W., Waring, K.M., Zimmermann, N.E., 2016. The impacts of increasing drought on forest dynamics, structure, and biodiversity in the United States. Glob. Change Biol. 22 (7), 2329–2352.

Cook, E.R., 1986. Users manual for program ARSTAN. Tree-ring chronologies of western North America: California, eastern Oregon and northern Great Basin.

Cook, E.R., Kairiukstis, L.A., 2013. Methods of Dendrochronology: Applications in the Environmental Sciences. Springer Science & Business Media.

Cook, E.R., Peters, K., 1981. The smoothing spline: a new approach to standardizing forest interior tree-ring width series for dendroclimatic studies.

Dang, H., Jiang, M., Zhang, Q., Zhang, Y., 2007. Growth responses of subalpine fir (Abies fargesii) to climate variability in the Qinling Mountain, China. For. Ecol. Manag. 240 (1), 143–150.

de Martonne, E., 1926. Une nouvelle function climatologique: l'indice d'aridité. Meteorologie 2, 449–459.

De Micco, V., Carrer, M., Rathgeber, C.B.K., Julio Camarero, J., Voltas, J., Cherubini, P., Battipaglia, G., 2019. From xylogenesis to tree rings: wood traits to investigate tree response to environmental changes. IAWA J. 40 (2), 155–182.

Dixon, P., 2003. VEGAN, a package of R functions for community ecology. J. Veg. Sci. 14 (6), 927–930.

Dusenge, M.E., Duarte, A.G., Way, D.A., 2019. Plant carbon metabolism and climate change: elevated $CO_2$ and temperature impacts on photosynthesis, photorespiration and respiration. New Phytol. 221 (1), 32–49.

Esper, J., Cook, E.R., Schweingruber, F.H., 2002. Low-frequency signals in long tree-ring chronologies for reconstructing past temperature variability. Science 295 (5563), 2250–2253 (1979).

Friedman, J.H., 1984. A Variable Span Smoother. Laboratory for Computational Statistics, Department of Statistics, Stanford.

Fritts, H., 2012. Tree Rings and Climate. Academic Press.

Fuchs, S., Schuldt, B., Leuschner, C., 2021. Identification of drought-tolerant tree species through climate sensitivity analysis of radial growth in Central European mixed broadleaf forests. For. Ecol. Manag. 494, 119287.

Führer, E., 2000. Forest functions, ecosystem stability and management. For. Ecol. Manag. 132 (1), 29–38.

Gao, D.X., Xaybouangeun, N., Zaw, Z., Yang, R.Q., Fan, Z.X., 2025. Growth resilience of Pinus latteri to extreme drought events across aridity gradients in southern Laos. Glob. Ecol. Conserv. 57, e03424.

Gao, S., Liu, R., Zhou, T., Fang, W., Yi, C., Lu, R., Zhao, X., Luo, H., 2018. Dynamic responses of tree-ring growth to multiple dimensions of drought. Glob. Change Biol. 24 (11), 5380–5390.

Gao, J., Yang, B., He, M., Shishov, V., 2019. Intra-annual stem radial increment patterns of Chinese pine, Helan Mountains, Northern Central China. Trees 33 (3), 751–763.

Gheyret, G., Zhang, H.T., Guo, Y., Liu, T.Y., Bai, Y.H., Li, S., Schmid, B., Bruelheide, H., Ma, K., Tang, Z., 2021. Radial growth response of trees to seasonal soil humidity in a subtropical forest. Basic Appl. Ecol. 55, 74–86.
Grimm, N.B., Chapin III, F.S., Bierwagen, B., Gonzalez, P., Groffman, P.M., Luo, Y., Melton, F., Nadelhoffer, K., Pairis, A., Raymond, P.A., Schimel, J., Williamson, C.E., 2013. The impacts of climate change on ecosystem structure and function. Front. Ecol. Environ. 11 (9), 474–482.
Grissino-Mayer, H.D., 2001. Evaluating crossdating accuracy: a manual and tutorial for the computer program COFECHA.
Hagerman, S.M., Pelai, R., 2018. Responding to climate change in forest management: two decades of recommendations. Front. Ecol. Environ. 16 (10), 579–587.
Hansen, M.C., Potapov, P.V., Moore, R., Hancher, M., Turubanova, S.A., Tyukavina, A., Thau, D., Stehman, S.V., Goetz, S.J., Loveland, T.R., Kommareddy, A., Egorov, A., Chini, L., Justice, C.O., Townshend, J.R.G., 2013. High-resolution global maps of 21st-century forest cover change. Science 342 (6160), 850–853 (1979).
Harris, I., Osborn, T.J., Jones, P., Lister, D., 2020. Version 4 of the CRU TS monthly high-resolution gridded multivariate climate dataset. Sci. Data 7 (1), 109.
He, M., Yang, B., Bräuning, A., 2013. Tree growth–climate relationships of Juniperus tibetica along an altitudinal gradient on the southern Tibetan Plateau. Trees 27 (2), 429–439.
He, S., Hao, C., 2024. Analysis on spatial-temporal variation characteristics of climate in Qinling-Huaihe demarcation zone since 1961. Ecol. Indic. 158, 111345.
Henttonen, H.M., Mäkinen, H., Heiskanen, J., Peltoniemi, M., Laurén, A., Hordo, M., 2014. Response of radial increment variation of Scots pine to temperature, precipitation and soil water content along a latitudinal gradient across Finland and Estonia. Agric. For. Meteorol. 198-199, 294–308.
Holmes, R.L., 1983. Computer assisted quality control in tree-ring dating and measurement. Tree-Ring Bull. 43, 69–78.
Huang, J., Tardif, J.C., Bergeron, Y., Denneler, B., Berninger, F., Girardin, M.P., 2010. Radial growth response of four dominant boreal tree species to climate along a latitudinal gradient in the eastern Canadian boreal forest. Glob. Change Biol. 16 (2), 711–731.
Huang, X., Dai, D., Xiang, Y., Yan, Z., Teng, M., Wang, P., Zhou, Z., Zeng, L., Xiao, W., 2021. Radial growth of Pinus massoniana is influenced by temperature, precipitation, and site conditions on the regional scale: a meta-analysis based on tree-ring width index. Ecol. Indic. 126, 107659.
Jentsch, A., von Heßberg, A., 2022. Disturbance regimes and climate extremes of the Earth's vegetation zones (Eds.). In: Wohlgemuth, T., Jentsch, A., Seidl, R. (Eds.), Disturbance Ecology. Springer International Publishing, Cham, pp. 41–75.
Kannenberg, S.A., Novick, K.A., Alexander, M.R., Maxwell, J.T., Moore, D.J.P., Phillips, R.P., Anderegg, W.R.L., 2019. Linking drought legacy effects across scales: from leaves to tree rings to ecosystems. Glob. Change Biol. 25 (9), 2978–2992.
King, G.M., Gugerli, F., Fonti, P., Frank, D.C., 2013. Tree growth response along an elevational gradient: climate or genetics? Oecologia 173 (4), 1587–1600.
Körner, C., 2003. Carbon limitation in trees. J. Ecol. 91 (1), 4–17.
Kou, Z.X., Yao, Y.H., Hu, Y.F., Zhang, B.P., 2020. Discussion on position of China's north-south transitional zone by comparative analysis of mountain altitudinal belts. J. Mt. Sci. 17 (8), 1901–1915.
Li, Q., Liu, Y., Song, H., Liu, R., Cai, Q., Sun, C., Fang, C., Cheng, H., 2023a. Sensitive climate response of tree-ring δ18O to current warming in the Qinling Mountains along a climate boundary in China. Clim. Dyn. 60 (9), 2597–2612.
Li, W., Jiang, Y., Dong, M., Du, E., Zhou, Z., Zhao, S., Xu, H., 2020. Diverse responses of radial growth to climate across the southern part of the Asian boreal forests in northeast China. For. Ecol. Manag. 458, 117759.
Li, W., Manzanedo, R.D., Jiang, Y., Ma, W., Du, E., Zhao, S., Rademacher, T., Dong, M., Xu, H., Kang, X., Wang, J., Wu, F., Cui, X., Pederson, N., 2023b. Reassessment of growth-climate relations indicates the potential for decline across Eurasian boreal larch forests. Nat. Commun. 14 (1), 3358.
Li, W., Zhu, L., Zhu, L., Jing, M., Qian, C., Zhu, Y., Cherubini, P., 2024. Old Pinus massoniana forests benefit more from recent rapid warming in humid subtropical areas of central-southern China. J. For. Res. 35 (1), 88 (Harbin).
Li, X., Ma, B., Lu, C., Yang, H., Sun, M., 2021. Spatial pattern and development of protected areas in the north-south transitional zone of China. Chin. Geogr. Sci. 31 (1), 149–166.
Liang, H., Huang, J.G., Ma, Q., Li, J., Wang, Z., Guo, X., Zhu, H., Jiang, S., Zhou, P., Yu, B., Luo, D., 2019. Contributions of competition and climate on radial growth of Pinus massoniana in subtropics of China. Agric. For. Meteorol. 274, 7–17.
Liu, G., Liu, H., Yin, Y., 2013a. Global patterns of NDVI-indicated vegetation extremes and their sensitivity to climate extremes. Environ. Res. Lett. 8 (2), 025009.
Liu, H., Park Williams, A., Allen, C.D., Guo, D., Wu, X., Anenkhonov, O.A., Liang, E., Sandanov, D.V., Yin, Y., Qi, Z., Badmaeva, N.K., 2013b. Rapid warming accelerates tree growth decline in semi-arid forests of Inner Asia. Glob. Change Biol. 19 (8), 2500–2510.
Lo, Y.H., Blanco, J.A., Seely, B., Welham, C., Kimmins, J.P., 2010. Relationships between climate and tree radial growth in interior British Columbia, Canada. For. Ecol. Manag. 259 (5), 932–942.
Lyu, L., Suvanto, S., Nöjd, P., Henttonen, H.M., Mäkinen, H., Zhang, Q.B., 2017. Tree growth and its climate signal along latitudinal and altitudinal gradients: comparison of tree rings between Finland and the Tibetan Plateau. Biogeosciences 14 (12), 3083–3095.
Ma, X., Chen, S., Zhang, Q., Li, Z., 2025. Contrasting responses of tree radial growth at different altitudes to climate warming in subtropical region of China. Ecol. Front. 45, 917–924.
Martin-Benito, D., Pederson, N., 2015. Convergence in drought stress, but a divergence of climatic drivers across a latitudinal gradient in a temperate broadleaf forest. J. Biogeogr. 42 (5), 925–937.
Martinez del Castillo, E., Zang, C.S., Buras, A., Hacket-Pain, A., Esper, J., Serrano-Notivoli, R., Hartl, C., Weigel, R., Klesse, S., Resco de Dios, V., Scharnweber, T., Dorado-Liñán, I., van der Maaten-Theunissen, M., van der Maaten, E., Jump, A., Mikac, S., Banzragch, B.E., Beck, W., Cavin, L., Claessens, H., Čada, V., Čufar, K., Dulamsuren, C., Gričar, J., Gil-Pelegrín, E., Janda, P., Kazimirovic, M., Kreyling, J., Latte, N., Leuschner, C., Longares, L.A., Menzel, A., Merela, M., Motta, R., Muffler, L., Nola, P., Petritan, A.M., Petritan, I.C., Prislan, P., Rubio-Cuadrado, Á., Rydval, M., Stajić, B., Svoboda, M., Toromani, E., Trotsiuk, V., Wilmking, M., Zlatanov, T., de Luis, M., 2022. Climate-change-driven growth decline of European beech forests. Commun. Biol. 5 (1), 163.
Maurya, J.P., Bhalerao, R.P., 2017. Photoperiod- and temperature-mediated control of growth cessation and dormancy in trees: a molecular perspective. Ann. Bot. 120 (3), 351–360.
Maxwell, R.S., Larsson, L.A., 2021. Measuring tree-ring widths using the CooRecorder software application. Dendrochronologia 67, 125841 (Verona).
Maynard, D.S., Bialic-Murphy, L., Zohner, C.M., Averill, C., van den Hoogen, J., Ma, H., Mo, L., Smith, G.R., Acosta, A.T.R., Aubin, I., Berenguer, E., Boonman, C.C.F., Catford, J.A., Cerabolini, B.E.L., Dias, A.S., González-Melo, A., Hietz, P., Lusk, C.H., Mori, A.S., Niinemets, Ü., Pillar, V.D., Pinho, B.X., Rosell, J.A., Schurr, F.M., Sheremetev, S.N., da Silva, A.C., Sosinski, Ê., van Bodegom, P.M., Weiher, E., Bönisch, G., Kattge, J., Crowther, T.W., 2022. Global relationships in tree functional traits. Nat. Commun. 13 (1), 3185.
McDowell, N.G., Allen, C.D., Anderson-Teixeira, K., Aukema, B.H., Bond-Lamberty, B., Chini, L., Clark, J.S., Dietze, M., Grossiord, C., Hanbury-Brown, A., Hurtt, G.C., Jackson, R.B., Johnson, D.J., Kueppers, L., Lichstein, J.W., Ogle, K., Poulter, B., Pugh, T.A.M., Seidl, R., Turner, M.G., Uriarte, M., Walker, A.P., Xu, C., 2020. Pervasive shifts in forest dynamics in a changing world. Science 368 (6494), eaaz9463 (1979).
McKown, A.D., Guy, R.D., Klápště, J., Geraldes, A., Friedmann, M., Cronk, Q.C., El-Kassaby, Y.A., Mansfield, S.D., Douglas, C.J., 2014. Geographical and environmental gradients shape phenotypic trait variation and genetic structure in Populus trichocarpa. New Phytol. 201 (4), 1263–1276.
Meinzer, F.C., Clearwater, M.J., Goldstein, G., 2001. Water transport in trees: current perspectives, new insights and some controversies. Environ. Exp. Bot. 45 (3), 239–262.
Meng, S., Fu, X., Zhao, B., Dai, X., Li, Q., Yang, F., Kou, L., Wang, H., 2021. Intra-annual radial growth and its climate response for Masson pine and Chinese fir in subtropical China. Trees 35 (6), 1817–1830.
Millar, C.I., Stephenson, N.L., Stephens, S.L., 2007. Climate change and forests of the future: managing in the face of uncertainty. Ecol. Appl. 17 (8), 2145–2151.
Mirabel, A., Girardin, M.P., Metsaranta, J., Way, D., Reich, P.B., 2023. Increasing atmospheric dryness reduces boreal forest tree growth. Nat. Commun. 14 (1), 6901.
Mountain Research Initiative EDW Working Group., 2015. Elevation-dependent warming in mountain regions of the world. Nat. Clim. Change 5, 424–430.
New, M., Lister, D., Hulme, M., Makin, I., 2002. A high-resolution data set of surface climate over global land areas. Clim. Res. 21 (1), 1–25.
Oliveira, R.S., Eller, C.B., Barros, F.D.V., Hirota, M., Brum, M., Bittencourt, P., 2021. Linking plant hydraulics and the fast–slow continuum to understand resilience to drought in tropical ecosystems. New Phytol. 230 (3), 904–923.
Pan, Y., Chen, J.M., Birdsey, R., McCullough, K., He, L., Deng, F., 2011. Age structure and disturbance legacy of North American forests. Biogeosciences 8 (3), 715–732.
Park Williams, A., Allen, C.D., Macalady, A.K., Griffin, D., Woodhouse, C.A., Meko, D.M., Swetnam, T.W., Rauscher, S.A., Seager, R., Grissino-Mayer, H.D., Dean, J.S., Cook, E. R., Gangodagamage, C., Cai, M., McDowell, N.G., 2013. Temperature as a potent driver of regional forest drought stress and tree mortality. Nat. Clim. Change 3 (3), 292–297.
Pau, S., Wolkovich, E.M., Cook, B.I., Davies, T.J., Kraft, N.J., Bolmgren, K., Betancourt, J. L., Cleland, E.E., 2011. Predicting phenology by integrating ecology, evolution and climate science. Glob. Change Biol. 17 (12), 3633–3643.
Peng, J., Yang, L., Peng, M., Wei, X., Li, J., Cui, J., Li, X., Li, J., 2023. Diverging growth and resilience of Pinus tabulaeformis and Pinus massoniana to droughts in north-south transition zone, central China. Dendrochronologia 78, 126060 (Verona).
Peng, K., Peng, J., Li, J., Li, J., Liu, Y., Li, J., Wei, X., 2025. Regional growth response and resilience of Pinus tabulaeformis to climate change in the north-south transition zone, central China. J. Plant Ecol.
Perry, D.A., Oren, R., Hart, S.C., 2008. Forest Ecosystems. Johns Hopkins University Press.
Roderick, M.L., Berry, S.L., 2001. Linking wood density with tree growth and environment: a theoretical analysis based on the motion of water. New Phytol. 149 (3), 473–485.
Seidl, R., Albrich, K., Thom, D., Rammer, W., 2018. Harnessing landscape heterogeneity for managing future disturbance risks in forest ecosystems. J. Environ. Manag. 209, 46–56.
Sidor, C.G., Popa, I., Vlad, R., Cherubini, P., 2015. Different tree-ring responses of Norway spruce to air temperature across an altitudinal gradient in the Eastern Carpathians (Romania). Trees 29 (4), 985–997.
Shi, X.Z., Yu, D.S., Warner, E.D., Pan, X.Z., Petersen, G.W., Gong, Z.G., Weindorf, D.C., 2004. Soil database of 1: 1000,000 digital soil survey and reference system of the Chinese genetic soil classification system. Soil Surv. Horiz. 45 (4), 129–136.
Song, Y., Jinfeng, W., Yong, G., Xu, C., 2020. An optimal parameters-based geographical detector model enhances geographic characteristics of explanatory variables for spatial heterogeneity analysis: cases with different types of spatial data. GIsci. Remote Sens. 57 (5), 593–610.
Speer, J.H., 2010. Fundamentals of Tree-Ring Research. University of Arizona Press.

Su, J., Gou, X., HilleRisLambers, J., Deng, Y., Fan, H., Zheng, W., Zhang, R., Manzanedo, R.D., 2021. Increasing climate sensitivity of subtropical conifers along an aridity gradient. For. Ecol. Manag. 482, 118841.
Tabakova, M.A., Arzac, A., Martínez, E., Kirdyanov, A.V., 2020. Climatic factors controlling Pinus sylvestris radial growth along a transect of increasing continentality in southern Siberia. Dendrochronologia 62, 125709 (Verona).
ter Braak, C.J.F., 1986. Canonical correspondence analysis: a new eigenvector technique for multivariate direct gradient analysis. Ecology 67 (5), 1167–1179.
Trugman, A.T., Anderegg, L.D., Wolfe, B.T., Birami, B., Ruehr, N.K., Detto, M., Bartlett, M.K., William, R.L., Anderegg, W.R., 2019. Climate and plant trait strategies determine tree carbon allocation to leaves and mediate future forest productivity. Glob. Change Biol. 25 (10), 3395–3405.
Tumajer, J., Scharnweber, T., Smiljanic, M., Wilmking, M., 2022. Limitation by vapour pressure deficit shapes different intra-annual growth patterns of diffuse- and ring-porous temperate broadleaves. New Phytol. 233 (6), 2429–2441.
Ullah, S., You, Q., Sachindra, D.A., Nowosad, M., Ullah, W., Bhatti, A.S., Jin, Z., Ali, A., 2022. Spatiotemporal changes in global aridity in terms of multiple aridity indices: an assessment based on the CRU data. Atmos. Res. 268, 105998.
van Mantgem, P.J., Stephenson, N.L., Byrne, J.C., Daniels, L.D., Franklin, J.F., Fulé, P.Z., Harmon, M.E., Larson, A.J., Smith, J.M., Taylor, A.H., Veblen, T.T., 2009. Widespread increase of tree mortality rates in the western United States. Science 323 (5913), 521–524 (1979).
Vilà-Cabrera, A., Martínez-Vilalta, J., Retana, J., 2015. Functional trait variation along environmental gradients in temperate and Mediterranean trees. Glob. Ecol. Biogeogr. 24 (12), 1377–1389.
Vitali, V., Büntgen, U., Bauhus, J., 2017. Silver fir and Douglas fir are more tolerant to extreme droughts than Norway spruce in south-western Germany. Glob. Change Biol. 23 (12), 5108–5119.
Wagner, S., Nocentini, S., Huth, F., Hoogstra-Klein, M., 2014. Forest management approaches for coping with the uncertainty of climate change trade-offs in service provisioning and adaptability. Ecol. Soc. 19, art32.
Wang, F., Arseneault, D., Pan, B., Liao, Q., Sugiyama, J., 2019. Pre-1930 unstable relationship between climate and tree-ring width of Pinus taiwanensis hayata in southeastern China. Dendrochronologia 57, 125629 (Verona).
Wang, J.F., Zhang, T.L., Fu, B.J., 2016. A measure of spatial stratified heterogeneity. Ecol. Indic. 67, 250–256.
Wang, S., Chen, F., Chen, Y., Torbenson, M.C.A., Esper, J., Zhao, X., Hu, M., Zhang, H., Yue, W., Cao, H., 2025. Greening of Eurasia's center driven by low-latitude climate warming. For. Ecosyst. 13, 100330.
Wang, L., Chen, S., Zhu, W., Ren, H., Zhang, L., Zhu, L., 2021. Spatiotemporal variations of extreme precipitation and its potential driving factors in China's North-South Transition Zone during 1960–2017. Atmos. Res. 252, 105429.
Wang, L., Fei, T., Bian, M., Xu, Y., Zhang, H., Zheng, Y., Zhu, H., 2022. Response of microscopical hyperspectral data to past climatic variable. Theor. Appl. Climatol. 150 (3), 1145–1155.
Waring, R.H., Running, S.W., 2010. Forest Ecosystems: Analysis at Multiple Scales. Academic Press.
Watson, J.E.M., Evans, T., Venter, O., Williams, B., Tulloch, A., Stewart, C., Thompson, I., Ray, J.C., Murray, K., Salazar, A., McAlpine, C., Potapov, P., Walston, J., Robinson, J.G., Painter, M., Wilkie, D., Filardi, C., Laurance, W.F., Houghton, R.A., Maxwell, S., Grantham, H., Samper, C., Wang, S., Laestadius, L., Runting, R.K., Silva-Chávez, G.A., Ervin, J., Lindenmayer, D., 2018. The exceptional value of intact forest ecosystems. Nat. Ecol. Evol. 2 (4), 599–610.
Way, D.A., 2011. Tree phenology responses to warming: spring forward, fall back? Tree Physiol. 31 (5), 469–471.
Wilmking, M., van der Maaten-Theunissen, M., van der Maaten, E., Scharnweber, T., Buras, A., Biermann, C., Gurskaya, M., Hallinger, M., Lange, J., Shetti, R., Smiljanic, M., Trouillier, M., 2020. Global assessment of relationships between climate and tree growth. Glob. Change Biol. 26 (6), 3212–3220.
Wilson, S.J., Cagalanan, D., 2016. Governing restoration: strategies, adaptations and innovations for tomorrow's forest landscapes. World Dev. Perspect. 4, 11–15.
Wu, X., Tang, W., Chen, F., Wang, S., Bakhtiyorov, Z., Liu, Y., Guan, Y., 2025. Attribution and risk projections of hydrological drought over water-scarce central asia. Earth's Future 13, e2024EF005243.
Xie, M., Cai, Q., Liu, Y., Ren, M., Zhou, Q., Zhang, H., Meng, K., 2024a. Assessing climatic response and drought resilience in growth of Pinus tabulaeformis Carr. And Tsuga chinensis Pritz. On the southern slope of the Qinling Mountains. Glob. Ecol. Conserv. 53, e02999.
Xie, Y., Shen, Z., Wang, T., Malanson, G.P., Peñuelas, J., Wang, X., Chen, X., Liang, E., Liu, H., Yang, M., Ying, L., Zhao, F., Piao, S., 2024b. Uppermost global tree elevations are primarily limited by low temperature or insufficient moisture. Glob. Change Biol. 30 (4), e17260.
Yan, B., Yu, J., Liu, Q., Wang, L., Hu, L., 2020. Tree-ring response of Larix chinensis on regional climate and sea-surface temperature variations in alpine timberline in the Qinling Mountains. J. For. Res. 31 (1), 209–218 (Harbin).
Yan, H., Zeng, X., Liu, X., Xue, Y., Li, Q., Zhang, L., Liu, J., 2026. Comparing ecological memory effects of the bimodal radial growth in the Qinling Mountains and Mediterranean forests. For. Ecosyst. 15, 100402.
Yue, W., Chen, F., Davi, N.K., Zhang, H., Chen, Y., Zhao, X., Gao, Z., 2024a. Little Ice Age cooling in the Western Hengduan Mountains, China: a 600-year warm-season temperature reconstruction from tree rings. Clim. Dyn. 62 (1), 773–790.
Yue, W., Torbenson, M.C.A., Chen, F., Reinig, F., Esper, J., Martinez del Castillo, E., Wang, S., Zhao, X., Hu, M., Xu, Y., Hadad, M.A., González-Reyes, Á., Roig, F.A., Hou, T., Cao, H., Wang, H., Zhang, H., Niu, J., Chen, Y., 2026. Runoff reconstructions and future projections indicate highly variable water supply from Pacific Rim water towers. AGU Adv. 7 (1), e2025AV002053.
Zang, C., Pretzsch, H., Rothe, A., 2012. Size-dependent responses to summer drought in Scots pine, Norway spruce and common oak. Trees 26 (2), 557–569.
Zhang, X., Zhang, B., Wang, J., Yu, F., Zhao, C., Yao, Y., 2021. North-south vegetation transition in the eastern Qinling-Daba Mountains. J. Geogr. Sci. 31 (3), 350–368.
Zhao, S., Jiang, Y., Wen, Y., Jiao, L., Li, W., Xu, H., Ding, M., 2021. Frequent locally absent rings indicate increased threats of extreme droughts to semi-arid Pinus tabuliformis forests in North China. Agric. For. Meteorol. 308-309, 108601.
Zhao, Y., Shi, J., Shi, S., Ma, X., Zhang, W., Wang, B., Sun, X., Lu, H., Bräuning, A., 2019a. Early summer hydroclimatic signals are captured well by tree-ring earlywood width in the eastern Qinling Mountains, central China. Clim. Past 15 (3), 1113–1131.
Zhao, Z., Fang, K., Cao, C., Chen, D., Liang, X., Dong, Z., Zhang, P., 2019b. Responses of the radial growth of the endangered species Keteleeria fortunei to climate change in southeastern China. Trees 33 (4), 977–985.
Zhao, Z., Kang, D., Guo, W., Zhao, L., Cui, L., Li, J., 2019c. Climate sensitivity of purple cone spruce (*Picea purpurea*) across an altitudinal gradient on the eastern Tibetan Plateau. Dendrochronologia 56, 125586 (Verona).
Zhu, W., Lu, Y., 2025. Spatio-temporal patterns and climatic drivers of spring phenology in eight forest communities across the north-south transitional zone of China. J. Geogr. Sci. 35 (1), 17–38.